Available online at www.sciencedirect.com
ScienceDirect
Journal of Sound and Vibration 311 (2008) 328–352
JOURNAL OF SOUND AND VIBRATION
www.elsevier.com/locate/jsvi

Analytical predictions of natural frequencies of cracked simply supported beams with a stationary roving mass

Shuncong Zhong, S. Olutunde Oyadiji*

Dynamics and Aeroelasticity Research Group, School of Mechanical, Aerospace and Civil Engineering, The University of Manchester, Manchester M13 9PL, UK

Received 10 March 2006; received in revised form 2 September 2007; accepted 12 September 2007
Available online 21 December 2007

Abstract

Natural frequencies of a damaged simply supported beam with a stationary roving mass are studied theoretically. The transverse deflection of the cracked beam is constructed by adding a polynomial function, which represents the effects of a crack, to the polynomial function which represents the response of the intact beam [J. Fernández-Sáez, L. Rubio, C. Navarro, Approximate calculation of the fundamental frequencies for bending vibrations of cracked beams, *Journal of Sound and Vibration* 225 (1999) 345–352]. By means of the boundary and kinematics conditions, approximate closed-form analytical expressions are derived for the natural frequencies of an arbitrary mode of transverse vibration of a cracked simply supported beam with a roving mass using the Rayleigh's method. The natural frequencies change due to the roving of the mass along the cracked beam. Therefore the roving mass can provide additional spatial information for damage detection of the beam. That is, the roving mass can be used to probe the dynamic characteristics of the beam by roving the mass from one end of the beam to the other. The presence of a crack causes the local stiffness of the beam to decrease which, in turn, causes a marked decrease in natural frequency of the beam when the roving mass is located in the vicinity of the crack. The magnitude of the roving mass used varied between 0% and 50% of the mass of the beam. The predicted frequencies are shown to compare very well with those obtained using the finite element method and the experimental results. Finally, the effects of crack depth, crack location and roving mass on the natural frequency of the beam are investigated. It is shown that the natural frequencies of the cracked beam decrease as the crack depth increases and as the roving mass is traversed closer to the crack location.

1. Introduction

Inspection of structural components for damage is vital for making decisions about their repair or retirement. A crack may cause serious failure of a structure; therefore it must be detected in the early state when it is small. In practice, it is difficult to recognize most cracks by using visual inspection techniques; generally, they may be detected by non-destructive techniques. System identification is an important tool for such purpose.

*Corresponding author. Tel.: +44 161 275 4348; fax: +44 161 275 3844.
E-mail address: s.o.oyadiji@manchester.ac.uk (S.O. Oyadiji).

0022-460X/$ - see front matter © 2007 Elsevier Ltd. All rights reserved.
doi:10.1016/j.jsv.2007.09.009

Nomenclature

A	cross-sectional area of the beam
B	width of beam
C_m	flexibility constant
E	Young's modulus of beam material
E_s	element size
f_b	frequency of the beam
f_{bm}	frequency of the beam with a roving mass
G	shear modulus of beam material
h_c	crack depth
H	depth of beam
I	the second moment of area of the beam's cross-section
l_c	location of a crack in the cracked beam from the left support of the beam
l_m	location of the roving mass from the left support of the beam
L	length of beam
m	roving mass
M	bending moment transmitted by the cracked section
M_b	mass of the cracked beam
R_{sh}	span-to-height ratio of beam
$S(h_c/H)$	configuration function for crack opening area
T_{max}	maximum kinetic energy
$U_{ci}(x)$	mode shape of the cracked beam for mode i
$U_{Ii}(x)$	mode shape of the intact beam for mode i
U_{max}	maximum potential energy
Δl	spatial interval of roving of mass along the cracked beam
$\Delta\Theta$	discontinuity in the slope of the beam
v	Poisson ratio of beam material
ρ	density of beam material
ψ_i	ratio of the frequency of the cracked beam with roving mass to the frequency of the cracked beam alone for mode i
ω	circular frequency of the beam
ω_{c1}	first natural angular frequency of the cracked beam with roving mass
ω_{c1}	variation of the first natural angular frequencies of the cracked beam with roving mass at the fixed location l_m
$\omega_{c1}(n)$	variation of the first natural angular frequencies of the cracked beam with roving mass at the different position n along the length of the beam
$\omega_{ci}(n)$	variation of the angular natural frequency of an arbitrary mode i of the cracked beam with roving mass at the different position n along the beam

In the last three decades, a lot of research effort has been devoted to develop effective approaches for detecting faults in machines and structures. This has resulted in a variety of analytical, numerical and experimental techniques. In an earlier critical review on the vibration of cracked structures [1], Dimarogonas discussed, in detail, various crack modelling methods including the equivalent reduced cross-section, local bending moment and the local flexibility methods, crack identifications in beams and rotors, and vibration coupling due to the presence of cracks. A wealth of further analytical, numerical and experimental investigations have been reviewed. Salawu [2] has presented a review of methods of damage detection using natural frequencies that are potentially useful for routine integrity assessment of structures. Frequency values obtained from periodic vibration testing can be used to monitor structural behaviour and also assess structural condition. An advantage of the approach is the global nature of the identified frequencies; thus allowing the measurement points to be selected. Wang et al. [3] reviewed the advances in detecting and locating damage in bridges by different kinds of non-destructive testing and evaluation (NDT & E) methods. From the application point of view, classifications for general bridge components and their damage types were presented. The relationships between damage, bridge components, and NDT & E techniques are summarized. A state-of-the-art review was presented by Zhou and Sim [4] regarding the research and development of *in situ* fibre-optic damage detection and assessment systems embedded in fibre-reinforced composite structures. Chang et al. [5] have given a review on health monitoring of civil infrastructure. The survey paper highlighted several research directions: the use of innovative signal processing, new sensor, and control theory. A recent paper presented by Carden and Fanning [6] reviewed the state of the art in vibration-based condition monitoring with particular emphasis on structural engineering applications.

Flaws or cracks in structures may have a serious influence on their dynamic characteristics. Cracks in structures produce local change in stiffness altering dynamic characteristics such as changes in mass distribution and damping properties. As a consequence, reduction in stiffness is associated with decreases in the natural frequencies and modification of the mode shape of the structure. In an earlier study, Chondros and Dimarogonas [7] had investigated the effects of cracks in welded joints using fracture mechanics concepts. The change in the bending stiffness of a beam due to a crack was measured and used in the mathematical model. They developed a frequency spectral method to identify cracks in various structures. However, due to the fact that the stress field induced by the crack decays with distance from the crack, a direct approach relating crack position and size with stiffness change is not easy to be developed. Such parameters affecting this approach were discussed in the papers of Chondros and Dimarogonas [8,9].

The detection of cracks based on measured vibration frequencies has been investigated by many authors. An earlier study carried out by Cawley and Adams [10] noted that the stress distribution through a vibrating cracked structure was non-uniform and was different for each natural frequency (mode). The authors stated that any localized damage would affect each mode differently, depending on the particular location of the damage. Consequently, the measurement of the natural frequencies of a structure at two or more stages of its lifetime offered the possibility of locating damage in any structure and of determining the severity of the damage. Narkis [11] indicated that the data on the variation of the first two natural frequencies is sufficient for identification of the location of a crack in a cracked simply supported uniform beam. Messina et al. [12,13] calculated the damage location assurance criterion, which was used to identify single defect and later extended to identify multiple damage sites on the basis of changes in the natural frequencies. A more comprehensive survey was presented later by Salawu [2]. This survey reviewed the numerous technical literatures available on crack detection based on the change in natural frequencies.

The ease of identification of natural frequencies has motivated the dynamic analysis of cracked structures. Some researchers are focused on calculation of natural frequencies of cracked structure. Christides and Barr [14] used a so-called two-term Rayleigh–Ritz solution to obtain the variation in the fundamental frequency of simply supported beams with a mid-span crack. However, on a closer examination of their work, their assumed mode shape is actually made up of the fundamental mode shape of a simply supported beam and a polynomial function which represents the effects of the crack. They evaluated only the fundamental frequency of the beam using the Rayleigh's quotient. Chondros et al. [15] developed a continuous cracked beam vibration theory for the lateral vibration of cracked Euler–Bernoulli beams with single- or double-edge open cracks. The crack was modelled as a continuous flexibility using the displacement field in the vicinity of the crack which was determined using fracture mechanics methods. The results of two independent evaluations of the lowest natural frequency of lateral vibration for beams with a single-edge crack were presented. Fernández-Sáez et al. [16] presented a simplified method to evaluate the fundamental frequency of cracked Euler–Bernouilli beams. The transverse deflection of the cracked beam was constructed by adding a polynomial function, which represents a crack, to the polynomial function of the intact beam. A closed-form expression for the fundamental frequency of a simply supported beam was given using Rayleigh's method.

Shen and Pierre [17] used an approximate Galerkin solution to analyse the free bending vibrations of simply supported cracked beams. An analytical approach to the fundamental frequency of cracked Euler–Bernoulli beams in bending vibrations is presented by Fernández-Sáez and Navarro [18]. The influence of the crack was represented by an elastic rotational spring connecting the two segments of the beam at the cracked section. Closed-form expressions for the approximated values of the fundamental frequency of cracked Euler–Bernoulli beams in bending vibration are given. The results obtained agree with those numerically obtained by the finite-element method (FEM). Loya et al. [19] have obtained the natural frequencies for bending vibrations of a Timoshenko cracked beam with simple boundary conditions (BCs). The beam was modelled as two segments connected by two massless springs (one extensional and the other rotational). Finally, simple expressions for the natural frequencies of simply supported cracked beams were obtained.

On the other hand, some solution methods for the fundamental natural frequency of intact beams with concentrated mass have been published. Low [20] used the equivalent-centre method to obtain the fundamental frequency of vibrating beams carrying a concentrated mass at various locations. Chai and Low [21] discussed proper shape functions to obtain high accuracy of fundamental natural frequency of slender uniform intact beams with a concentrated mass. De Rosa et al. [22] examined the dynamic behaviour of a

slender beam carrying a concentrated mass at an arbitrary abscissa, and the resulting frequency equation was numerically solved. Low [23] presented a frequency analysis of an Euler–Bernoulli intact beam carrying a concentrated mass at an arbitrary location. The dimensionless frequency equation for 10 combinations of classical BCs was obtained by satisfying the differential equation of motion and by imposing the corresponding boundary and compatibility conditions. Then Low [24] found that the eigenfrequency can be predicted for an individual beam system carrying a single mass, by virtue of the Dunkerley's formula. Also, the Dunkerley's method was recommended by Low for a beam carrying more than two masses at different positions. Low [25,26] investigated the methods to derive frequency equations of intact beams carrying multiple masses. In Ref. [25], Low compared the method of frequency determinant and the method of Laplace transform for the effectiveness of each derivation for the frequency equation of the same beam-mass system. Low [26] applied the method of Rayleigh quotient together with the respective shape function with a simple trigonometric function for a quick frequency estimation of the beam-mass system.

During the period of vibration of a cracked structural member, the crack does not always remain open. The static defection due to some loading component on the cracked beam (residual loads, body weight of a structure, etc.), combined with the vibration effect may cause the crack to open at all times, or open and close regularly, or to completely close depending on various loads at a given time. Chondros et al. [27] stated that if the static defection due to some loading component on the beam (dead loads, own weight, etc.), is larger than the vibration amplitudes, then the crack remains open all the time, or opens and closes regularly and the problem is linear. If the static defection is small, then the crack will open and close in time depending on the vibration amplitude. In this case the system is nonlinear. Chondros et al. [27] also discussed the effect of a breathing crack on the flexural vibration of cracked structures. It should be noted that the crack model in the present work always remains open during vibration. Therefore, the complexities associated with the nonlinear characteristics due to a breathing crack are not present in this work.

Several researchers have investigated the effects of cracks on structures subjected to a moving load. Mahmoud and Abou Zaid [28] developed an iterative modal analysis approach to determine the effect of transverse cracks on the dynamic behaviour of simply supported undamped Bernoulli–Euler beams subject to a moving mass. The presence of a crack results in higher deflections and alters the beam response patterns. In particular, the largest defection in the beam for a given speed takes longer to build up, and a discontinuity appears in the slope deflected shape of the beam at the crack location. Crack effects become more noticeable as crack depth increases. The effect of the inertia force due to the moving mass is, in general, qualitatively similar and additive to the effect of the crack. The exact effect of crack and mass depends on the speed, time, crack size, crack location, and the moving mass magnitude. Lin and Chang [29] developed an analytical method to present the dynamic response of a cracked cantilever beam subject to a concentrated moving load. The cracked beam system is modelled as a two-span beam and each span of the continuous beam is assumed to obey Euler–Bernoulli beam theory. The crack is modelled as a rotational spring with sectional flexibility. Considering the compatibility requirements on the crack, the relationships between these two spans can be obtained. By using the analytical transfer matrix method, eigensolutions of this cracked system are obtained explicitly. The forced responses can be obtained by modal expansion theory using the determined eigenfunctions. Some numerical results are shown to present the crack effects (crack extent, location of the crack) and were studied for different speeds of the moving load.

As mentioned before, researchers have focused on the study of the frequency analysis of intact beams with moving masses. In the present work, the frequency estimation of cracked beams with a stationary roving mass is investigated. The transverse deflection of the cracked beam is constructed by adding a polynomial function, which represents the effects of the crack, to the polynomial function which represents the response function of the intact beam [16]. This paper presents a closed-form analytical expression for calculating frequencies of a cracked simply supported beam with a roving mass. The classical application of the Rayleigh's method to determine the fundamental frequency of vibrations is extended to higher modes in order to derive approximate formulae for evaluating the natural frequencies of a beam traversed by a stationary roving mass. But it should be noted that this extension of the Rayleigh's method is not the same as the Rayleigh–Ritz method which requires the use of shape functions that contain the behaviour of the modes of interest to determine their natural frequencies and mode shapes simultaneously. The extension of Rayleigh's method in this work is the determination of the Rayleigh's quotient for each mode of vibration of a cracked beam using a modified form

of the corresponding mode shape of an intact beam as the shape function. The results calculated from the closed-form equation compare very well with those obtained by FEM and experimental results. Six masses of magnitudes between 0% and 50% of the mass of the beam are used to show the effect of mass and location on the natural frequency change. The roving mass which is traversed along the beam provides new approaches for crack detection in beam-like structures.

It should be noted here that this proposed method based on a stationary roving mass is different from the moving mass (or moving load) methods published in Refs. [28,29]. Mahmoud and Abou Zaid [28] and Lin and Chang [29] have investigated deflections (or mode shapes) of structures (simply supported beams and cantilever beams) subjected to a moving mass (or moving load) of a fixed or variable velocity. However, the proposed method in this paper is focused on investigation of natural frequencies of cracked beams subjected to a roving mass which is stationary (zero velocity) at each location considered. The roving of the mass enhances the effects of the crack on the dynamics of the beam and facilitates the identification and location of damage in the beam. The phrase 'stationary roving mass' has been used in preference to 'moving mass' in order to highlight the fact that in this paper the mass is stationary at each location. Therefore, the method proposed here does not consider a mass with a given velocity.

2. Formulation of cracked simply supported beam

The equation of motion of a uniform intact beam subjected to free harmonic vibration is given by [30–33]

$$EI\frac{\mathrm{d}^4U_I}{\mathrm{d}x^4}(x)-\rho A\omega^2U_I(x)=0, \tag{1}$$

where E is Young's modulus and I is the second moment of area of the beam's cross-section, ω is the circular frequency of the beam, $U_I(x)$ is the arbitrary scaled deformation term, x is the independent spatial variable, ρ is mass density, and A is cross-sectional area of the beam. It should be noted that this elementary Euler–Bernoulli theory of transverse vibrations of beams does not include the effects of rotary inertia and transverse shear displacement.

The general solution of Eq. (1) and its spatial derivatives are given by [30–33]

$$U_I(x)=A_1\cosh\beta x+A_2\sinh\beta x+A_3\cos\beta x+A_4\sin\beta x, \tag{2}$$

$$\frac{\mathrm{d}U_I}{\mathrm{d}x}=\beta(A_1\sinh\beta x+A_2\cosh\beta x-A_3\sin\beta x+A_4\cos\beta x), \tag{3}$$

$$\frac{\mathrm{d}^2U_I}{\mathrm{d}x^2}=\beta^2(A_1\cosh\beta x+A_2\sinh\beta x-A_3\cos\beta x-A_4\sin\beta x), \tag{4}$$

where A_1–A_4 are arbitrary constants which need to be determined from the BCs. For a simply supported beam, both displacement and bending moment will be zero at each end. Accordingly, one has the following modal BCs:

$$U_I(0)=U_I(L)=\frac{\mathrm{d}^2U_I}{\mathrm{d}x^2}(0)=\frac{\mathrm{d}^2U_I}{\mathrm{d}x^2}(L)=0, \tag{5}$$

where L is the length of beam. Substituting Eq. (5) into Eqs. (3) and (4), gives the equations for the circular frequency ω_i and mode shape U_{Ii} as [30–33]

$$\omega_i=(i\pi/L)^2\sqrt{\frac{EI}{\rho A}}\ \text{for } i=1,2,3,\ldots, \tag{6}$$

$$U_{Ii}(x)=D_i\sin\left(\frac{i\pi x}{L}\right)\ \text{for } i=1,2,3,\ldots, \tag{7}$$

where D_i is an arbitrary scaling constant.

3. Formulation of cracked simply supported beam with roving mass

3.1. Derivation of transverse deflected shape of cracked beam

A simply supported beam carrying a roving mass with a single-sided transverse crack whose depth is h_c, is shown in Fig. 1. The crack is located at position $x = l_c$ from the left support of the beam. The width, depth and length of the beam are, respectively, B, H and L, while m is the roving mass which is located at position $x = l_m$. The crack is assumed to be fully opened throughout the period of vibration and the effect of the crack is very apparent only at the crack location. The presence of the crack introduces a discontinuity or change in the slope of the beam at the crack location which can be expressed as [16]

$$\Delta\Theta = C_m M, \tag{8}$$

where M is the bending moment transmitted by the cracked section and C_m is the flexibility constant given by

$$C_m = \frac{H}{EI} S\left(\frac{h_c}{H}, \text{cross-section geometry}\right). \tag{9}$$

As the cross-section is rectangular, then the function $S(h_c/H)$, which is the configuration function for crack opening area, can be evaluated by fracture mechanics as [16,34]

$$S(h_c/H) = 2\left(\frac{h_c/H}{1-h_c/H}\right)^2 \left[5.93 - 19.69(h_c/H) + 37.14(h_c/H)^2 - 35.84(h_c/H)^3 + 13.12(h_c/H)^4\right]. \tag{10}$$

The transverse deflected shape U_{ci} for any mode i of the cracked beam can be obtained from that of the intact beam $U_{Ii}(x)$ by including a cubic polynomial function $B(x) = B_0 + B_1x + B_2x^2 + B_3x^3$ to represent the effects of the crack on the displacement of the section of the cracked beam located to the left of the crack, and another polynomial function $C(x) = C_0 + C_1x + C_2x^2 + C_3x^3$ to represent crack effects on displacement of the section of the beam to the right of the crack. Thus [16],

$$U_{ci}(x) = \begin{cases} U_{c1i}(x) = U_{Ii}(x) + B_0 + B_1x + B_2x^2 + B_3x^3, & 0 \leqslant x \leqslant l_c \\ U_{c2i}(x) = U_{Ii}(x) + C_0 + C_1x + C_2x^2 + C_3x^3, & l_c \leqslant x \leqslant L \end{cases} \text{for } i = 1, 2, 3, \ldots, \tag{11}$$

where the eight unknowns B_j and $C_j (j = 0,1,\ldots,3)$ are to be determined from the boundary and kinematics conditions of the two beam segments. Already, Eq. (11) satisfies the BCs, which are expressed by Eq. (5), while the kinematics conditions are given by

$$U_{c1i}(l_c) = U_{c2i}(l_c), \quad \frac{d^2U_{c1i}(l_c)}{dx^2} = \frac{d^2U_{c2i}(l_c)}{dx^2}, \quad \frac{d^3U_{c1i}(l_c)}{dx^3} = \frac{d^3U_{c2i}(l_c)}{dx^3}, \tag{12}$$

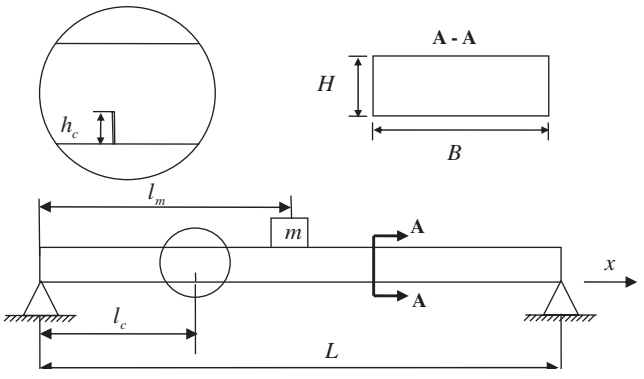

Fig. 1. Model of a cracked simply supported beam with auxiliary mass.

$$\Delta\Theta = \frac{\mathrm{d}U_{c2i}(l_c)}{\mathrm{d}x} - \frac{\mathrm{d}U_{c1i}(l_c)}{\mathrm{d}x} = HS(h_c/H)\frac{\mathrm{d}^2U_{c2i}(l_c)}{\mathrm{d}x^2}. \tag{13}$$

For the fundamental mode of vibrations, that is for the case $i=1$, Eq. (7) gives $U_{I1}(x) = D_1 \sin(\pi x/L)$. Using this result in Eqs. (5), (11), (12) and (13) and simplifying gives $U_{c1}(x)$ as

$$U_{c1}(x) = \begin{cases} U_{c11}(x) = U_{I1}(x) - D_1\dfrac{\pi^2 l_c H}{L^2}\left(1-\dfrac{L}{l_c}\right)S(h_c/H)\dfrac{x}{L}\sin\dfrac{\pi l_c}{L}, & 0 \leqslant x \leqslant l_c, \\ U_{c12}(x) = U_{I1}(x) + D_1\dfrac{\pi^2 l_c H}{L^2}S(h_c/H)\left(1-\dfrac{x}{L}\right)\sin\dfrac{\pi l_c}{L}, & l_c \leqslant x \leqslant L. \end{cases} \tag{14}$$

3.2. Derivation of approximate formulae for fundamental frequency of cracked beam with roving mass

Generally, the fundamental frequency can be obtained by Rayleigh's method [30–33]. The maximum values of kinetic energy $T_{\max}$ and potential energy $U_{\max}$ of the cracked simply supported beam can be calculated as

$$T_{\max} = \frac{\rho A\omega_{c1}^2}{2}\left[\int_0^{l_c} U_{c11}^2(x)\,\mathrm{d}x + \int_{l_c}^{L} U_{c21}^2(x)\,\mathrm{d}x\right] + \frac{1}{2}m\omega_{c1}^2 U_{c1}^2(l_m), \tag{15}$$

$$U_{\max} = \frac{EI}{2}\left[\int_0^{l_c}\left(\frac{\mathrm{d}^2U_{c11}(x)}{\mathrm{d}x^2}\right)^2\mathrm{d}x + \int_{l_c}^{L}\left(\frac{\mathrm{d}^2U_{c21}(x)}{\mathrm{d}x^2}\right)^2\mathrm{d}x\right] + \frac{1}{2}\Delta\Theta\, M, \tag{16}$$

where l_m is the location of the roving mass from the left support of the beam. It should be noted here that it has been assumed that the transverse deflected shape of a cracked beam with a roving mass is approximately the same as the case of cracked beam without a roving mass. In reality, the mode shapes of an intact beam with a roving mass are different from those of an intact beam without a roving mass, as shown in Refs. [21,23–26]. However, when the magnitude of the roving mass is relatively small, the mode shapes of an intact beam with a roving mass are similar to those of intact beams without roving masses.

The Rayleigh's formula for the fundamental frequency is derived by equating the maximum values of kinetic and potential energy. Thus, from Eqs. (15) and (16), the first natural angular frequency of the cracked beam with roving mass at the location l_m can be obtained as

$$\omega_{c1}^2 = \frac{EI\left[\int_0^{l_c}\left(\dfrac{\mathrm{d}^2U_{c11}(x)}{\mathrm{d}x^2}\right)^2\mathrm{d}x + \int_{l_c}^{L}\left(\dfrac{\mathrm{d}^2U_{c21}(x)}{\mathrm{d}x^2}\right)^2\mathrm{d}x\right] + (1/2)\Delta\Theta\, M}{\rho A[\int_0^{l_c} U_{c11}^2(x)\,\mathrm{d}x + \int_{l_c}^{L} U_{c21}^2(x)\,\mathrm{d}x] + (1/2)mU_{c1}^2(l_m)}. \tag{17}$$

This expression was evaluated using the Mathematica symbolic algebra software to give the first natural angular frequency. When the roving mass traverses along the cracked beam at the interval of Δl, the variation of the first natural angular frequency $\omega_{c1}(n)$ with position n along the length of the cracked beam can be expressed as

$$\omega_{c1}(n) = \omega_1\left[\frac{1+\eta\gamma_1}{1+2\eta\gamma_1 + (\pi^4/3)\eta^2[(l_c/L)^4\gamma_1 - 2(l_c/L)^3\gamma_1 + ((l_c/L)^2\gamma_1)] + \alpha_1'(n)}\right]^{1/2}, \tag{18}$$

where

$$\eta = \left(\frac{H}{L}\right)S\left(\frac{h_c}{H}\right), \tag{19}$$

$$\gamma_1 = 1 - \cos(2\pi l_c/L), \tag{20}$$

$$\alpha_1'(n) = \frac{2mU_{c1}^2(l_m)}{D_1^2\rho AL}, \tag{21}$$

$$l_m = n\,\Delta l, \quad n = 0, 1, 2, \ldots, \frac{L}{\Delta l} + 1, \tag{22}$$

$$\omega_1 = (\pi/L)^2 \sqrt{\frac{EI}{\rho A}}. \tag{23}$$

The detail derivation of Eq. (18) can be found in the appendix. It should be noted that Eq. (23) is obtained from Eq. (6) for the case $i = 1$, which is the first circular natural frequency of the intact beam.

3.3. Derivation of approximate formulae for higher frequencies of cracked beam with roving mass

Similarly, assuming that the Rayleigh's quotient can be applied to higher modes of vibration and following the above procedure, the variation of the angular natural frequency of an arbitrary mode i of the simply supported cracked beam with position of the roving mass along the beam can be expressed as

$$\omega_{ci}(n) = \omega_i \left[\frac{1 + \eta\gamma_i}{1 + 2\eta\gamma_i + (i^4\pi^4/3)\eta^2[(l_c/L)^4\gamma_i - 2(l_c/L)^3\gamma_i + ((l_c/L)^2\gamma_i)] + \alpha_i'(n)} \right]^{1/2}, \tag{25}$$

where

$$\gamma_i = 1 - \cos(2\pi i l_c/L), \tag{26}$$

$$\alpha_i'(n) = \frac{2mU_{ci}^2(n\,\Delta l)}{D_i^2 \rho A L}, \quad n = 0, 1, 2, \ldots, \frac{L}{\Delta l} + 1, \tag{27}$$

$$U_{ci}(x) = \begin{cases} U_{ci1}(x) = U_{Ii}(x) - D_i \dfrac{i^2\pi^2 l_c H}{L^2}\left(1 - \dfrac{L}{l_c}\right) S(h_c/H)\dfrac{x}{L}\sin\dfrac{i\pi l_c}{L}, & 0 \leqslant x \leqslant l_c, \\ U_{ci2}(x) = U_{Ii}(x) + D_i \dfrac{i^2\pi^2 l_c H}{L^2} S(h_c/H)\left(1 - \dfrac{x}{L}\right)\sin\dfrac{i\pi l_c}{L}, & l_c \leqslant x \leqslant L. \end{cases} \tag{28}$$

4. Numerical simulations, experimental verification and discussion of results

In this paper, a simply supported cracked beam was studied by the proposed analytical method and the FEM. The beam with a single-sided transverse crack of depth h_c, and located at distance l_c from the left support is shown in Fig. 1. The width, depth and length of the beam are, respectively, B, H and L.

4.1. Comparison of natural frequencies obtained from different FE models

It is noted here that indiscriminate application of the frequencies calculated by FEM, without consideration of the assumptions under which the crack or flaw models were derived and are valid, might lead to gross errors. In this subsection, the simply supported cracked beam was studied using the ABAQUS FE code [36]. FE models consisting of one- (1D), two- (2D) and three-dimensional (3D) models of a cracked beam were analysed. A single-sided transverse crack with a depth $h_c = 5$ mm was located at 500 mm from the left end of the cracked beam. All the cracked beam models were made of a bright mild steel of cross-sectional area $100 \times 25\,\text{mm}^2$ with a length of 3000 mm. It has the following material properties: Young's modulus $E = 210$ GPa, Shear modulus $G = 80$ GPa, density $\rho = 7850\,\text{kg/m}^3$, and Poisson ratio $v = 0.3$. The natural frequencies of the first 20 vibration bending modes of the cracked beam were computed by performing eigenvalue extraction using ABAQUS.

Fig. 2 shows three FE models of the cracked beam. For 1D FE mesh, as shown in Fig. 2(a), the element type was the 3-node beam element which is denoted in ABAQUS FE package as B22. Four different axial lengths of elements ($l_x = 5$, 25, 125 and 250 mm) were used in the analysis, which resulted in 601, 121, 25, and 13

nodes, respectively, in the FE model for a 3000 mm long cracked beam. The element B22 has three degrees of freedom (two translations in x- and y-axis, one rotation around z-axis) at the nodes. This 1D FE model considers the effect of rotary inertia and transverse shear. The crack is modelled by FE using a slot of width 1 mm and located where the arrow is shown in Fig. 2(a). The profile of the beam section is a rectangle of 100×25 mm except that the profile at the cracked area is a $100 \times 20\,\text{mm}^2$ rectangle.

Fig. 2(b) and (c) are, respectively, the 2D and 3D FE mesh used in the analysis. The 2D FE model used the eight-node plane stress element CPS8R while the 20-node 3D brick element C3D20R was used for the 3D FE model. Similarly, four different axial lengths of elements ($l_x = 5$, 25, 125 and 250 mm) were used in the 2D and 3D FE models. The element CPS8R has two degrees of freedom (two translations in x- and y-axis). The element C3D20R has three degrees of freedom (three translations in x-, y- and z-axis). The 3D FE model considers the effects of rotary inertia and transverse shear but these effects are neglected in the 2D FE model. In the 2D FE model, a slot of 1 mm wide × 5 mm deep simulated the 5 mm deep crack, while the 3D FE model used a slot of $1 \times 5 \times 100\,\text{mm}^3$. The locations of these slots are indicated by the arrows shown in Fig. 2(b) and (c).

Fig. 3(a)–(d) show the variations of the natural frequencies of the cracked beam with the number of the bending mode using the above three FE models when four element lengths ($l_x = 5$, 25, 125 and 250 mm) were used. It can be seen from Fig. 3 that the natural frequencies are almost the same when the element length is small (i.e. $l_x = 5$, 25 mm) or the number of bending mode is small (i.e. the first eight bending modes). However, for the higher modes, the frequencies are different due to the inclusion or non-inclusion of the effects of rotary inertia and transverse shear.

In this paper, the first four natural frequencies of bending vibration were employed in the comparisons between the proposed analytical method and the FEM. Therefore, since the first four natural frequencies obtained from the 1D, 2D and 3D FE models are almost the same, then any of these FE models can be used. But in order to model cracks which are angled in the $x-y$ or $x-z$ planes, only 3D model can be used. Consequently, the 3D model was selected for all FE analysis.

4.2. Comparisons of analytical and FE results of a cracked beam with roving mass

The model of the cracked beam is the same as the above 3D FE model. Only the element length of 5 mm was used for analysis. Six types of roving mass ratios were used, namely: $m/M_b = 1.1\%$, 2.1%, 4.2%, 6.4%, 8.5%, and 10.6%. The spatial interval of roving mass along the beam is 25 mm. The natural frequencies of the first four vibration bending modes of the cracked beam were computed by performing eigenvalue extraction and comparing the results with the proposed analytical result obtained from Eq. (25).

Fig. 4(a) shows the variation of the frequency ratio of the first mode with non-dimensional axial location of the roving mass. The figure shows the comparison of the results obtained using the proposed analytical method with those obtained using the FEM when the six roving masses were traversed along the length of the cracked beam at a spatial interval of 25 mm. As can be seen from Fig. 4(a), the ranges of the first natural frequency ratios are increased when the magnitude of the roving mass is increased. For example, the range of the first natural frequency ratios of the cracked beam with auxiliary mass ratio $m/M_b = 1.1\%$ is from 1.0 to 0.989, while the range for $m/M_b = 10.6\%$ is from 1.0 to 0.908. Fig. 4(b) shows the relative deviation between the predictions of the analytical and FEM for the variations of the first natural frequency for different roving

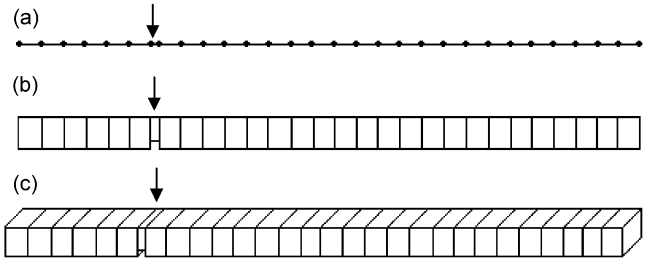

Fig. 2. FE models of a cracked beam ($l_c/L = 1/6$, $L = 3$ mm, $h_c = 5$ mm): (a) 1D model, (b) 2D model, and (c) 3D model.

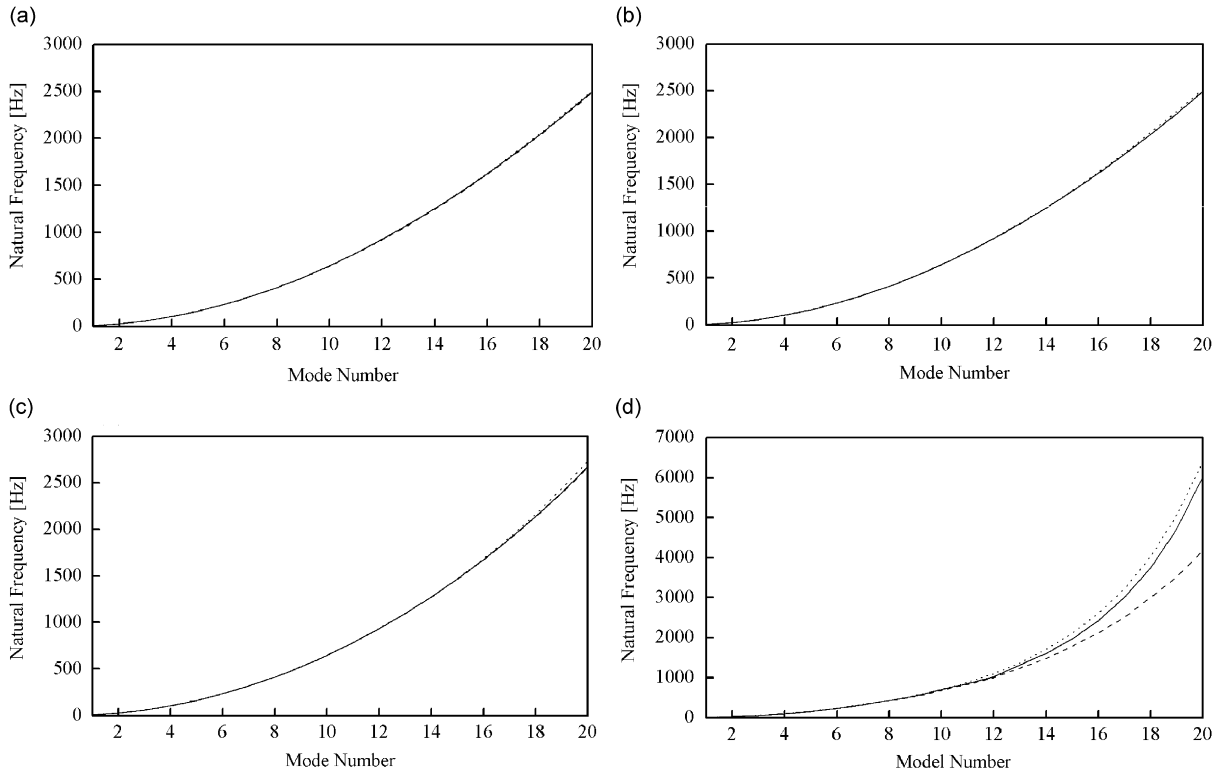

Fig. 3. Natural frequencies of the cracked beam ($l_c/L = 1/6$, $L = 3$ mm, $h_c = 5$ mm) with the number of bending mode using the three FE models with different element length (l_x): (———) 1D model, (– – – –) 2D model, (· · · · ·) 3D model for (a) $l_x = 5$ mm, (b) $l_x = 25$ mm, (c) $l_x = 125$ mm, and (d) $l_x = 250$ mm.

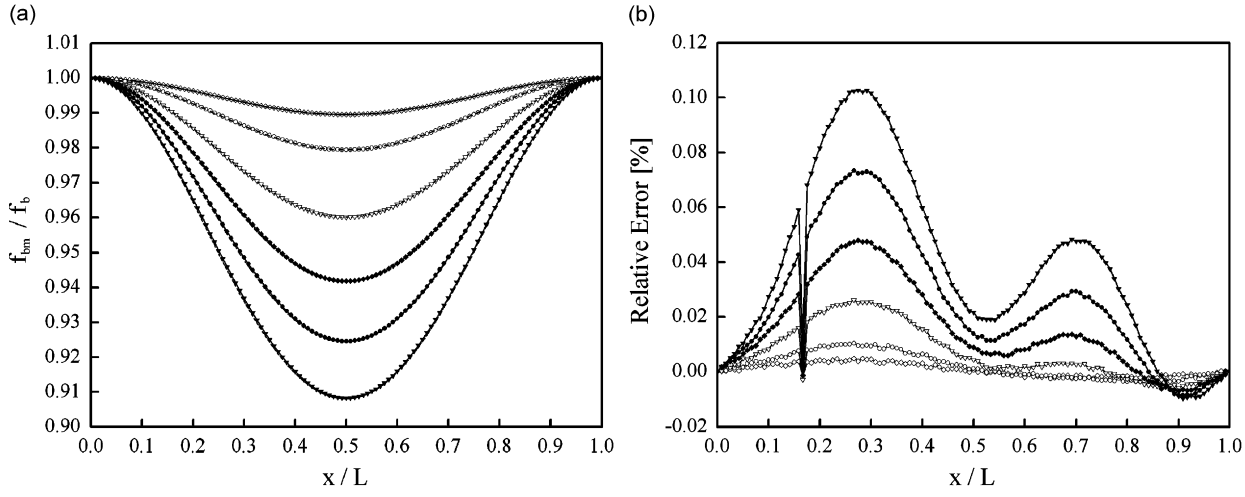

Fig. 4. Comparison of the predicted variation of frequency ratio f_{bm}/f_b (a) of the first mode of the cracked beam ($l_c/L = 1/6$, $h_c/H = 20\%$) with non-dimensional axial location x/L of the auxiliary mass and the relative deviation (b) between the proposed analytical method (AM) and the finite element method (FEM): (—◇—) AM, (———) FEM, $m/M_b = 1.1\%$; (—○—) AM, (– – – –) FEM, $m/M_b = 2.1\%$; (—▽—) AM, (· · · · ·) FEM, $m/M_b = 4.2\%$; (—◆—) AM, (–·–·–·) FEM, $m/M_b = 6.4\%$; (—●—) AM, (–··–··–) FEM, $m/M_b = 8.5\%$; (—▼—) AM, (·····) FEM, $m/M_b = 10.6\%$.

masses. It is seen that the maximum absolute deviation between the two sets of predictions is less than 0.12%. Therefore, the estimated values of the first natural frequency ratios of the cracked beam with roving mass using the analytical equation are very close to those obtained from FE calculations.

Fig. 5 shows the difference between the frequencies of the cracked beam with the roving mass in different positions from 10% to 50% of the length of the beam and the frequency of the cracked beam alone for mode 1. As can be seen from Fig. 5, when the position of the roving mass and the magnitude of the roving mass are increased, the difference is also increased. The relationship between the difference between the frequencies and the magnitude of the roving mass is almost linear. For example, when the roving mass ratio is 10.6% and the location of the roving mass is only 10% from the left end of the beam, Fig. 5 shows that the difference in frequencies is less than 1.0%. But when the roving mass ratio is 10.6% and the mass is located at the centre of the beam (50% of the length of the beam), the difference in frequencies is about 9.0%. Similarly, it is seen that for all values of roving mass, the greatest difference in frequency occurs when the mass is located at the centre of the beam. This is due to the fact that the centre of the beam is the antinode of the first mode of the beam and a roving mass positioned at that location has the greatest effect. In addition, Fig. 5 shows that there is a very good agreement between the analytical and FE predictions.

Figs. 6(a), 8(a), and 10(a) are, respectively, the variation of the frequency ratios of the second, third, and fourth modes with non-dimensional axial location of the roving mass. The figures show the comparison of the results obtained using the proposed analytical method with those obtained using the FEM when the six roving masses are traversed along the length of the cracked beam at a spatial interval of 25 mm. Figs. 6(b), 8(b), and 10(b) are the corresponding relative deviations between the predictions of the proposed analytical and FEM for the variations of the natural frequencies of the second, third and fourth modes for different roving masses. These figures show that the relative deviations are increased when the magnitude of the roving mass and the mode number are increased. For example, the maximum relative deviation of mode 2 is less than 1.2% whereas those of modes 3 and 4 are, respectively, less than 2.4% and less than 3.4%. Therefore, all the estimated values of the natural frequencies of the cracked beam with roving mass using the proposed analytical method are very close to those obtained from FE calculations when the magnitude of the roving mass is less than 11% of the mass of the beam (Figs. 7–11).

Similarly, Figs. 7, 9 and 11 show the corresponding differences between the frequencies of the cracked beam with the roving mass in different positions ranging from 10% to 50% of the length of the beam and the frequency of the cracked beam alone for modes 2–4. As can be seen from these figures, when the magnitude of the roving mass is increased, the difference is also increased but in a fairly nonlinear fashion. Also, when the position of the roving mass is increased, the difference is changed in a different way from that for mode 1. For example, the difference for mode 2 is increased when the position of the roving mass is traversed from 10% to

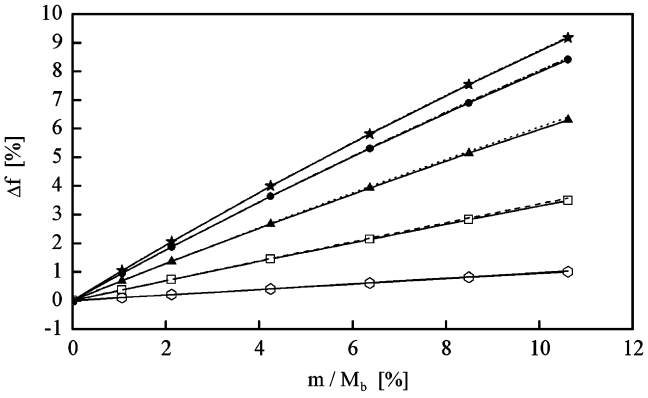

Fig. 5. Comparison of the difference between the predicted frequencies of the first mode of the cracked beam ($l_c/L = 1/6$, $h_c/H = 20\%$) with auxiliary mass and the frequency of the cracked beam alone for varying auxiliary mass ratios and varying locations of the auxiliary mass using the proposed method (AM) and the finite element method (FEM): (———) FEM, (—○—) AM, $l_m/L = 0.1$; (– – – –) FEM, (—□—) AM, $l_m/L = 0.2$; (· · · · ·) FEM, (—▲—) AM, $l_m/L = 0.3$; (–· –· –·) FEM, (—●—) AM, $l_m/L = 0.4$; and (–·· –·· –·) FEM, (—★—) AM, $l_m/L = 0.5$.

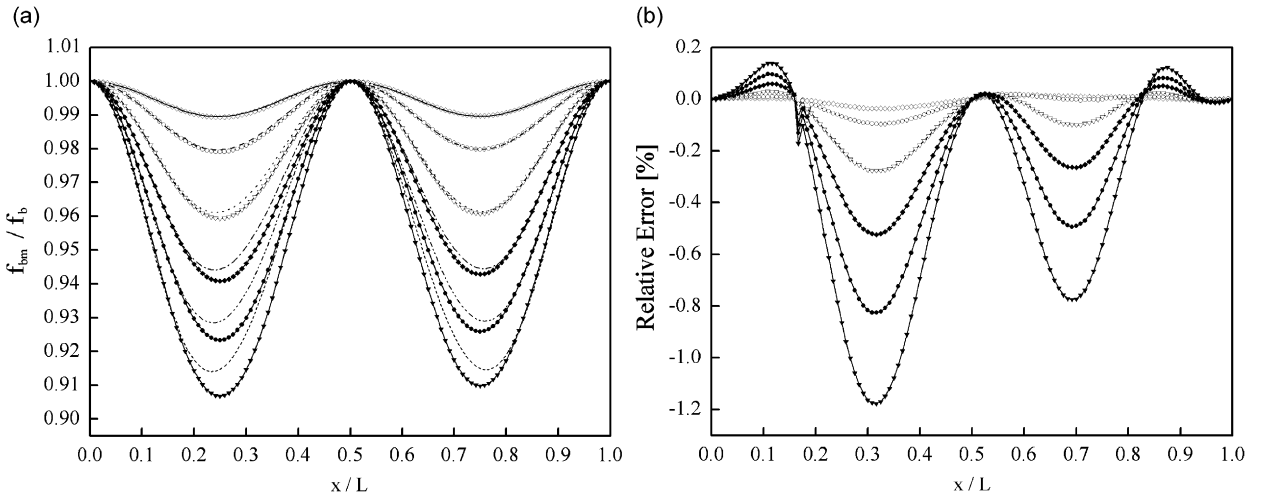

Fig. 6. Comparison of the predicted variation of frequency ratio f_{bm}/f_b (a) of the second mode of the cracked beam ($l_c/L = 1/6$, $h_c/H = 20\%$) with non-dimensional axial location x/L of the auxiliary mass and the relative deviation (b) between the proposed analytical method (AM) and the finite element method (FEM): (—◇—) AM, (————) FEM, $m/M_b = 1.1\%$; (—◇—) AM, (– – – –) FEM, $m/M_b = 2.1\%$; (—▽—) AM, (· · · · ·) FEM, $m/M_b = 4.2\%$; (—●—) AM, (–· –· –) FEM, $m/M_b = 6.4\%$; (—●—) AM, (–·· –·· –) FEM, $m/M_b = 8.5\%$; and (—▼—) AM, (·····) FEM, $m/M_b = 10.6\%$.

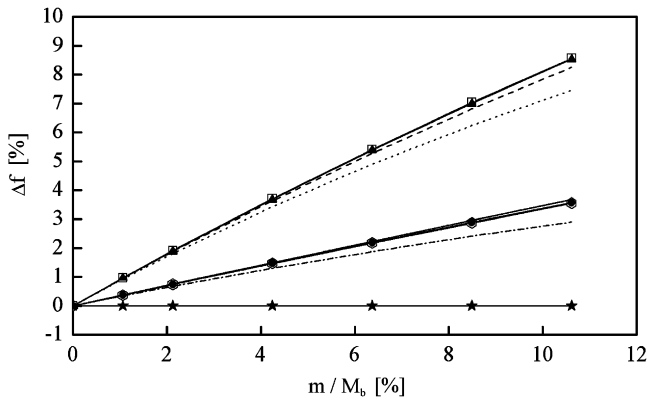

Fig. 7. Comparison of the difference between the predicted frequencies of the second mode of the cracked beam ($l_c/L = 1/6$, $h_c/H = 20\%$) with auxiliary mass and the frequency of the cracked beam alone for varying auxiliary mass ratios and varying locations of the auxiliary mass using the proposed method (AM) and the finite element method (FEM): (————) FEM, (—○—) AM, $l_m/L = 0.1$; (– – – –) FEM, (—□—) AM, $l_m/L = 0.2$; (· · · · ·) FEM, (—▲—) AM, $l_m/L = 0.3$; (–· –· –) FEM, (—●—) AM, $l_m/L = 0.4$; and (–·· –·· –) FEM, (—★—) AM, $l_m/L = 0.5$.

20% of the length of the beam whereas the difference is decreased when the position of the roving mass is traversed from 30% to 50% length of the beam. When the roving mass is located at the positions of 20% and 30% length of the beam, the differences of these two cases are almost the same. But when the mass is located at the centre of the beam, the difference between the frequencies of the cracked and intact beams is zero. This behaviour, which results in the banding of the curves into three groups as shown in Fig. 7, is due to the fact that mode 2 has a nodal position at the centre of the beam. Therefore, when the roving mass is located at the centre of the beam, there is no difference in frequency as can clearly seen from Fig. 6(a). Also, when the roving mass is near one end or near the centre, the difference in frequencies is small. But when the roving mass is located between 20% and 30% of the length of beam, the largest difference in frequencies are observed. This is due to the antinodal position of mode 2 that exists at 25% of the beam length. The variations observed in Figs. 9 and 11 for modes 3 and 4 can similarly be explained in terms of the corresponding nodal and antinodal positions.

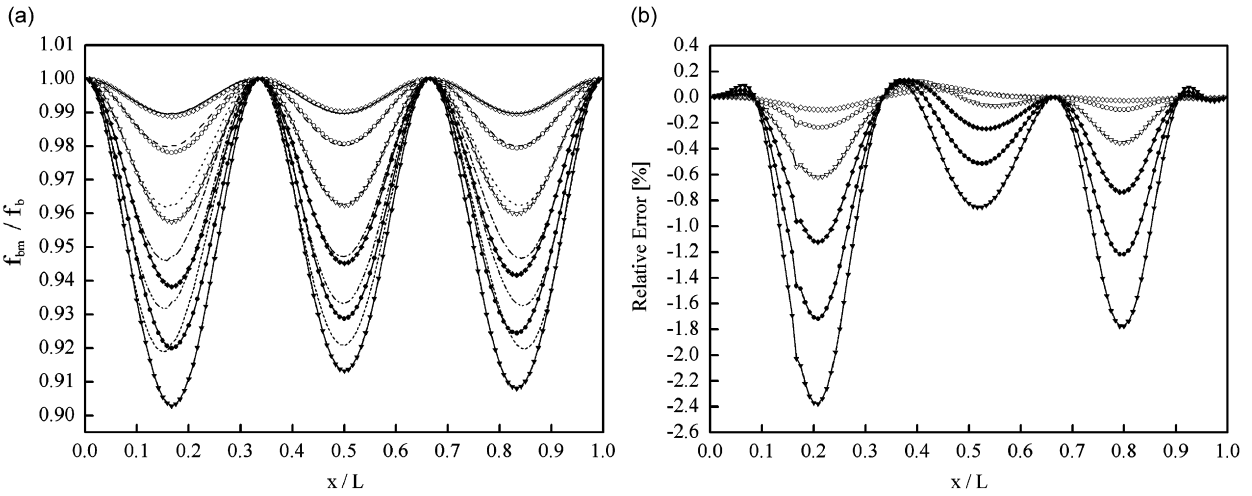

Fig. 8. Comparison of the predicted variation of frequency ratio f_{bm}/f_b (a) of the third mode of the cracked beam ($l_c/L = 1/6$, $h_c/H = 20\%$) with non-dimensional axial location x/L of the auxiliary mass and the relative deviation (b) between the proposed analytical method (AM) and the finite element method (FEM): (—◇—) AM, (————) FEM, $m/M_b = 1.1\%$; (—○—) AM, (– – – –) FEM, $m/M_b = 2.1\%$; (—▽—) AM, (· · · · · ·) FEM, $m/M_b = 4.2\%$; (—●—) AM, (–·–·–·) FEM, $m/M_b = 6.4\%$; (—●—) AM, (–··–··–) FEM, $m/M_b = 8.5\%$; and (—▼—) AM, (·····) FEM, $m/M_b = 10.6\%$.

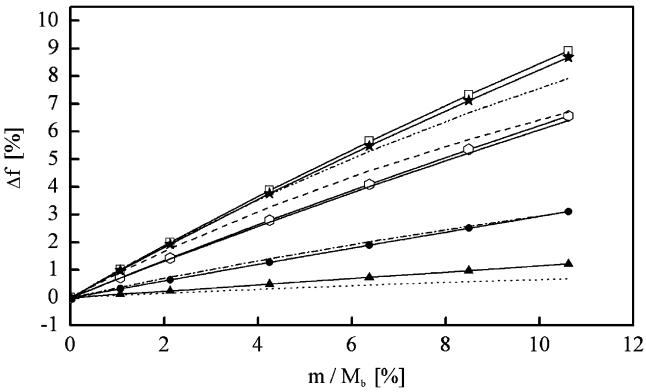

Fig. 9. Comparison of the difference between the predicted frequencies of the third mode of the cracked beam ($l_c/L = 1/6$, $h_c/H = 20\%$) with auxiliary mass and the frequency of the cracked beam alone for varying auxiliary mass ratios and varying locations of the auxiliary mass using the proposed method (AM) and the finite element method (FEM): (————) FEM, (—○—) AM, $l_m/L = 0.1$; (– – – –) FEM, (—□—) AM, $l_m/L = 0.2$; (· · · · · ·) FEM, (—▲—) AM, $l_m/L = 0.3$; (–·–·–·) FEM, (—●—) AM, $l_m/L = 0.4$; and (–··–··–) FEM, (—★—) AM, $l_m/L = 0.5$.

4.3. Comparisons of analytical and FE results for beams with different span-to-height ratios

All the previous results were obtained from beams with a span-to-height ratio R_{sh} of 120 ($R_{sh} = L/H = 3000\,\text{mm}/25\,\text{mm} = 120$). This subsection analyses the cases for small span-to-height ratios of 30 and 50, i.e., the length of the beams are 750 and 1250 mm, respectively. Fig. 12(a-1)–(d-1) show the variations of the first four frequency ratios of the cracked beam ($R_{sh} = 50$, $h_c = 5\,\text{mm}$) with non-dimensional axial location of the roving mass. The crack location ratio is $l_c/L = 0.4$ while the roving mass ratio is $m/M_b = 2.1\%$.

Fig. 12(a-2)–(d-2) show the relative deviation between the predictions of the analytical and FEM for the variations of the first four natural frequencies. It is seen that the maximum absolute deviation between the two sets of predictions for the first mode is less than 0.11%. The maximum absolute deviations for the second, third and fourth modes are, respectively, less than 0.6%, 0.8% and 1.5%. Therefore, the estimated values of

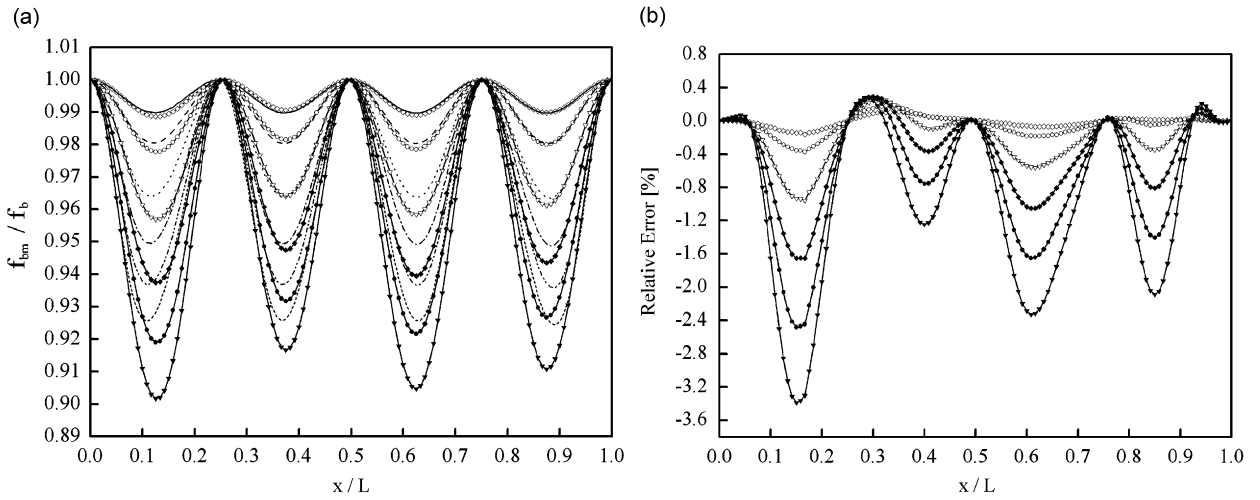

Fig. 10. Comparison of the predicted variation of frequency ratio f_{bm}/f_b (a) of the fourth mode of the cracked beam ($l_c/L = 1/6$, $h_c/H = 20\%$) with non-dimensional axial location x/L of the auxiliary mass and the relative deviation (b) between the proposed analytical method (AM) and the finite element method (FEM): (—◇—) AM, (————) FEM, $m/M_b = 1.1\%$; (—○—) AM, (– – – –) FEM, $m/M_b = 2.1\%$; (—▽—) AM, (· · · · · ·) FEM, $m/M_b = 4.2\%$; (—◆—) AM, (–· –· –·) FEM, $m/M_b = 6.4\%$; (—●—) AM, (–·· –·· –··) FEM, $m/M_b = 8.5\%$; and (—▼—) AM, (·····) FEM, $m/M_b = 10.6\%$.

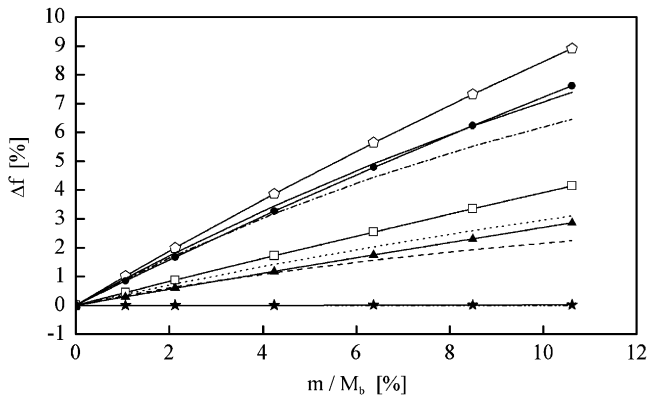

Fig. 11. Comparison of the difference between the predicted frequencies of the fourth mode of the cracked beam ($l_c/L = 1/6$, $h_c/H = 20\%$) with auxiliary mass and the frequency of the cracked beam alone for varying auxiliary mass ratios and varying locations of the auxiliary mass using the proposed method (AM) and the finite element method (FEM): (————) FEM, (—○—) AM, $l_m/L = 0.1$; (– – – –) FEM, (—□—) AM, $l_m/L = 0.2$; (· · · · · ·) FEM, (—▲—) AM, $l_m/L = 0.3$; (–· –· –·) FEM, (—●—) AM, $l_m/L = 0.4$; and (–·· –·· –··) FEM, (—★—) AM, $l_m/L = 0.5$.

the first four natural frequency ratios of the cracked beam with roving mass using the analytical equation are very close to those obtained from FE calculations when the span-to-height ratio R_{sh} is 50. However, it can be seen from Figs. 4, 6, 8 and 10 that the maximum relative deviations of the first four modes for a beam with a span-to-height of 120 are, respectively, less than 0.01%, 0.1%, 0.2% and 0.4%. Hence, the relative deviations are increased when the span-to-height ratio of a beam is decreased. The conclusion can be also verified by the results shown in Fig. 13 which shows the variation of the first four frequency ratios, and the corresponding relative deviations between the predictions of the analytical and FEM for the variations of the first four natural frequencies when the span-to-height ratio R_{sh} is 30. The maximum relative deviations of the first four modes are increased to 0.3%, 1.4%, 1.8% and 3.8%.

The reason for these phenomena is that the analytical method in the paper is based on the Euler–Bernoulli beam theory which does not include the effects of rotary inertia and shear deformation. But if the

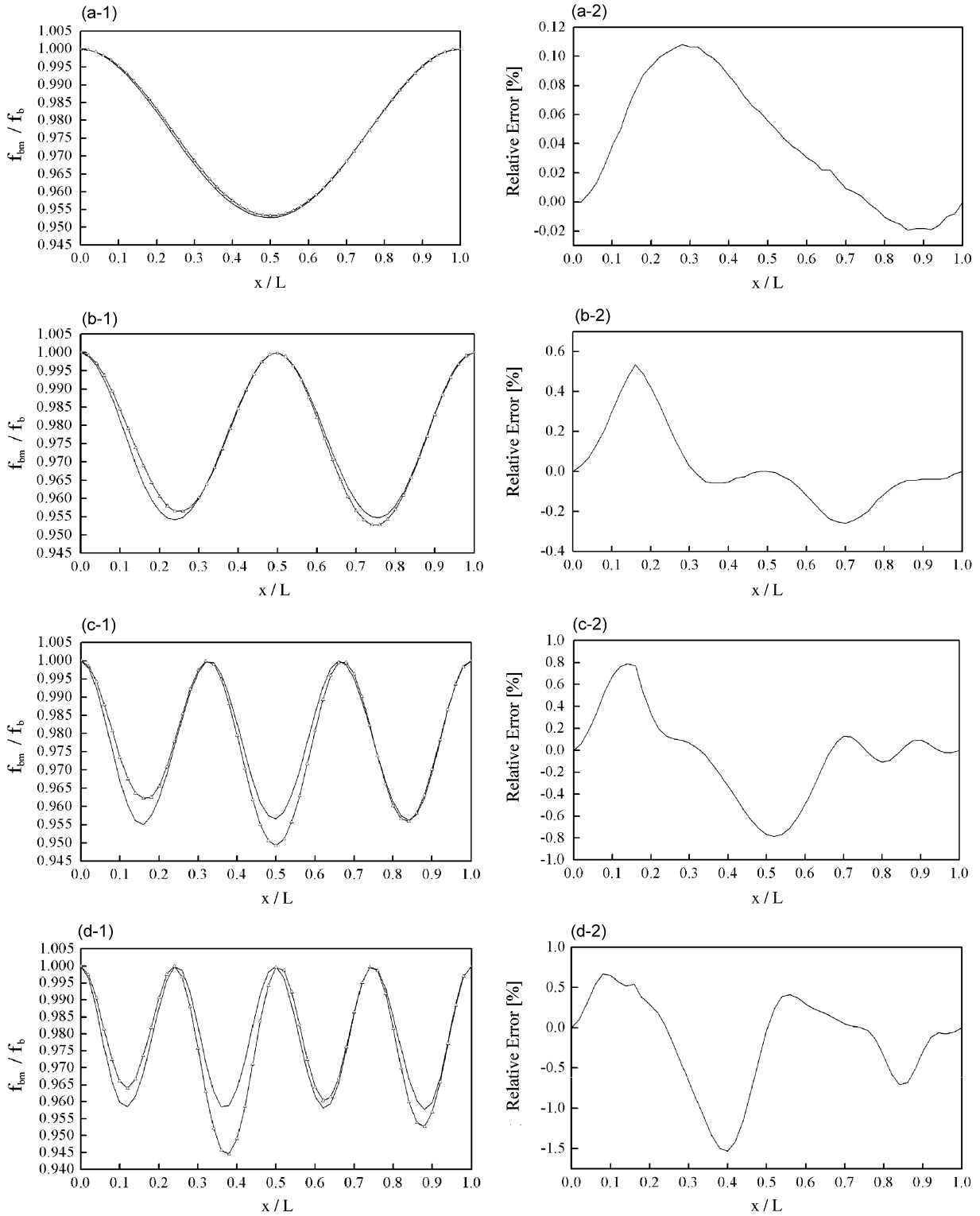

Fig. 12. Comparison of the predicted variation of frequency ratio f_{bm}/f_b of the first four modes of the cracked beam ($l_c/L = 1/6$, $R_{sh} = 50$) with non-dimensional axial location x/L of the auxiliary mass ($m/M_b = 2.1\%$) and the relative deviation between the proposed analytical method (AM) and the finite element method (FEM): (—△—) AM, (————) FEM for (a) mode 1, (b) mode 2, (c) mode 3 and (d) mode 4.

span-to-height ratio is decreased, the rotary inertia and the shear deformation effects will become more significant. For these same reasons, the error is also significant in the calculation of natural frequencies of vibration at higher modes [35]. A future work on the method based on the use of the Timoshenko beam model, which includes the effects of rotary inertia and shear deformation, will be studied to provide a more accurate method for all cracked beams with different span-to-height ratios.

4.4. Experimental verification

Experimental tests using simply supported aluminium beams were conducted. The dimensions of the damaged beam are $L \times H \times B = 2400 \times 25 \times 100\,\text{mm}^3$, and the crack, whose depth is 5 mm, was located at $l_c = 0.4\,\text{m}$ and was cut by a steel saw. The mass of the damaged beam is 16.2 kg. Fig. 14 shows the experimental set-up used for testing. A random signal was generated by the LMS experimental modal testing system, then amplified by a power amplifier, and exerted on the beam structure through a shaker. The response signal and input signal were, respectively, sensed by a PCB accelerometer and a PCB force sensor. The spatial probing interval of the roving mass was 100 mm which resulted in a total of 25 positions of the roving mass along the cracked beam. The frequency response functions (FRFs) of the cracked beam with two different roving masses $m = 2$ and 4 kg were measured and the natural frequencies were derived using the LMS testing system. The roving mass ratios (m/M_b) are, respectively, 12.3% and 25% for the case of $m = 2$ and 4 kg.

Fig. 15(a-1) and (a-2) are, respectively, the first two natural frequency curves of a cracked beam with the two different roving masses, which were obtained by experiment and analytical predictions. Fig. 15(b-1) and (b-2) are the corresponding maximum relative deviations of the first two modes. From Fig. 15(a-1) and (b-1), there is a very good agreement between the analytical and experimental results for the first natural frequency. For example, the maximum relative deviation is less than 0.4% for the case of $m = 2$ kg, and is less than 0.8% for the case of $m = 4$ kg. For the second mode, the maximum relative deviation is less than 1.0% for the case of $m = 2$ kg, and is less than 4.2% for the case of $m = 4$ kg. Therefore, the relative deviation is increased when the magnitude of the roving mass and the mode number are increased. However, in a real application, the magnitude of mass should be limited to a low value (i.e. 20%) to avoid destroying the beam-like structure itself. Therefore, the predicted frequencies obtained from Eq. (25) are very useful in real applications.

4.5. Effect of crack depth and crack location

Fig. 16(a)–(d) show the variations of the first four frequency ratios of the cracked beam with non-dimensional axial location of the roving mass. The crack location ratio is $l_c/L = 0.4$ while the roving mass ratio is 4.2%. Depths of cracks ranging from 0% to 50% are investigated. In fact, an intact beam with a roving mass is a special case whose crack depth is 0%. As can be seen from these figures, the frequencies are decreased when the crack depth is increased, i.e., the differences of frequencies between cracked beams and intact beam with roving mass are larger when the crack is deeper. Also, the higher the mode, the greater the difference in frequencies. Thus, for crack depths of 50%, Fig. 17 shows that the largest differences in frequencies are about 5%, 7%, 12%, and 15% for modes 1–4, respectively.

In Fig. 17(a)–(d) is shown the variations of the first four frequency ratios of the cracked beam with non-dimensional axial location of the roving mass. In this case, the crack depth ratio h_c/H is 50% whereas the roving mass ratio is 4.2%. The results shown are for six crack location ratios of $l_c/L = 1/12$, 2/12, 3/12, 4/12, 5/12, 6/12 which are designated by numbers 2–7, respectively. The intact beam is designated by number 1. The results show that when the crack location ratios change from $l_c/L = 1/12$ to 6/12, the variations of the frequency ratios of different modes change in a different way. For mode 1, when the crack location ratio is increased from $l_c/L = 1/12$ to 6/12, the frequency ratio is decreased. However, for the second to fourth modes, the changes of the frequency ratios are related to the existence of nodes and the amplitudes of mode shapes, which are shown in Fig. 20. For mode 2, the frequency ratio is decreased from $l_c/L = 1/12$ to 3/12 and is increased from $l_c/L = 3/12$ to 6/12. This is because mode 2 has a node at position $l_c/L = 6/12$ and an antinode (maximum amplitude of mode shape) at position $l_c/L = 3/12$. Also, the crack effect is larger when the amplitude of the mode shape is larger.

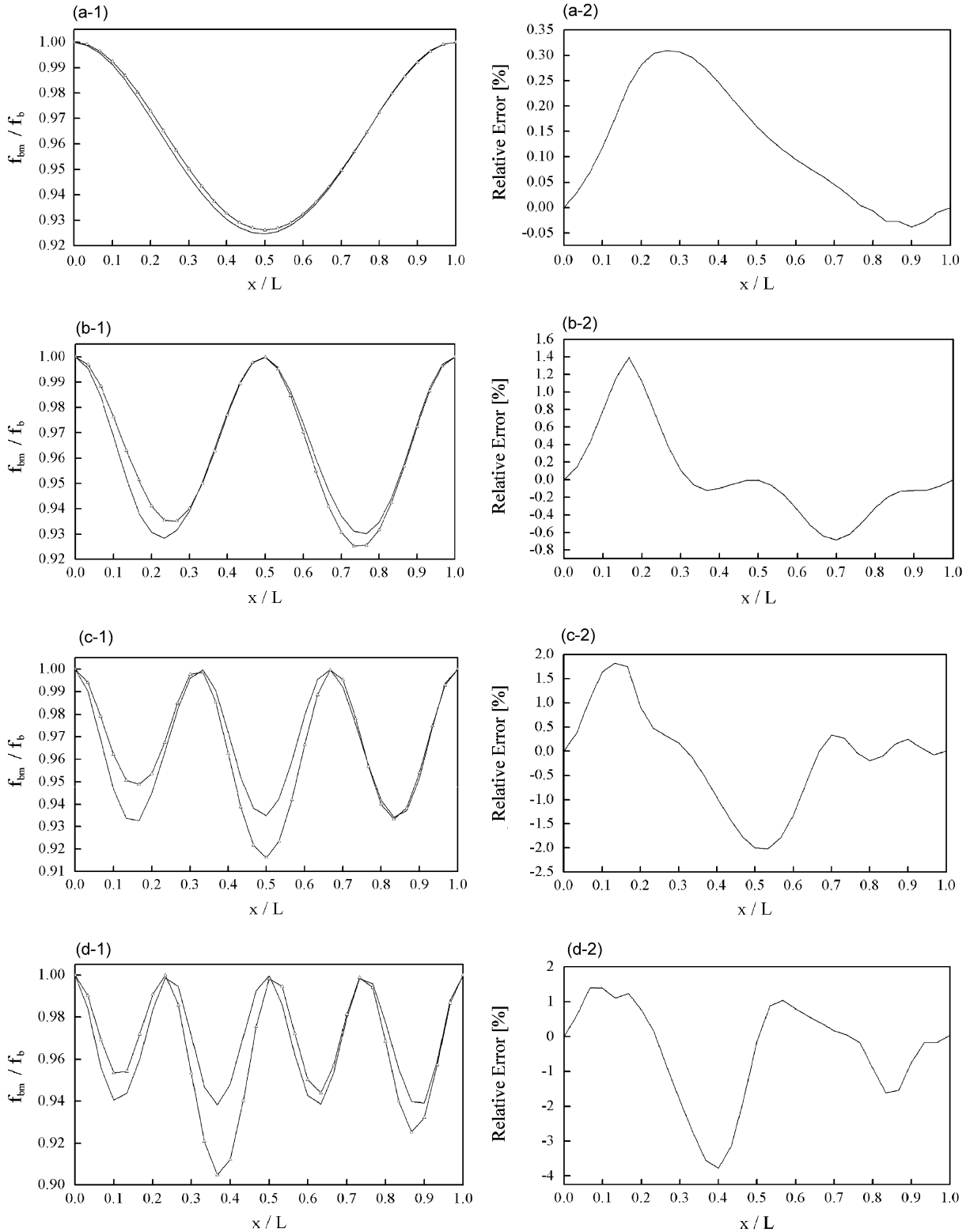

Fig. 13. Comparison of the predicted variation of frequency ratio f_{bm}/f_b of the first four modes of the cracked beam ($l_c/L = 1/6$, $R_{sh} = 30$) with non-dimensional axial location x/L of the auxiliary mass ($m/M_b = 2.1\%$ $m/M_b = 2.1\%$) and the relative deviation between the proposed analytical method (AM) and the finite element method (FEM): (—△—) AM, (————) FEM for (a) mode 1, (b) mode 2, (c) mode 3 and (d) mode 4.

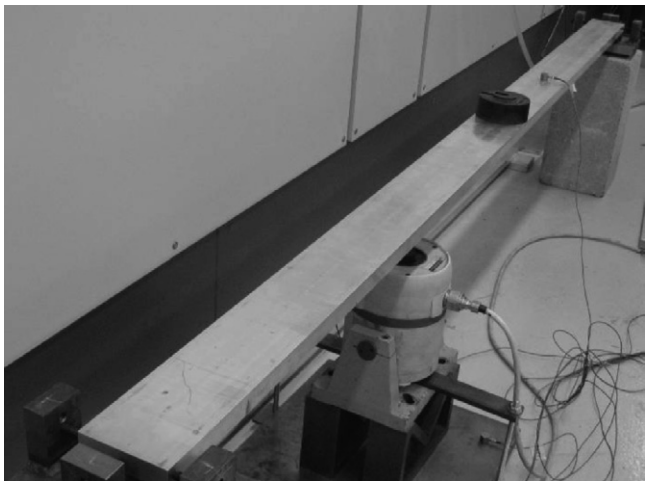

Fig. 14. Experimental setup.

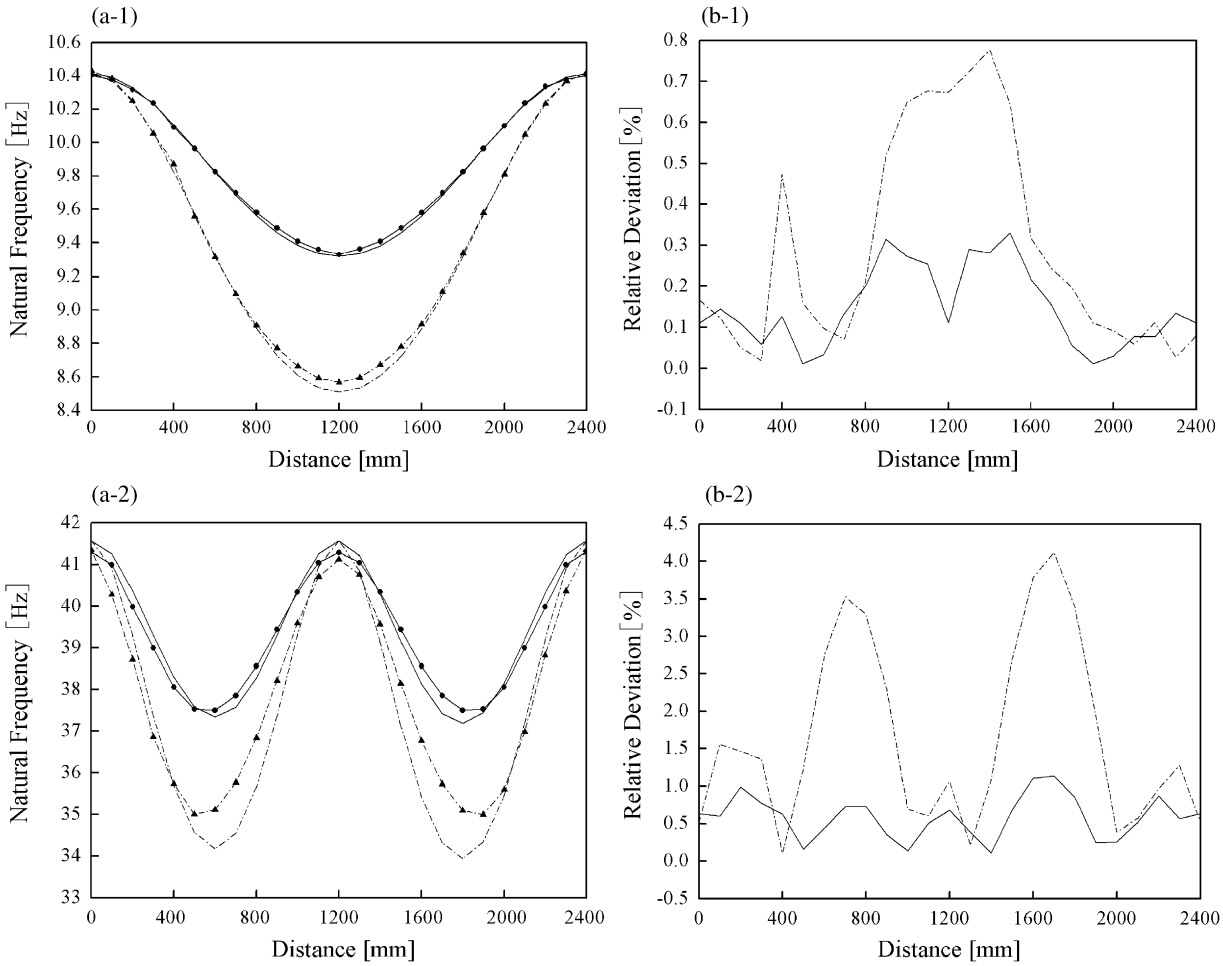

Fig. 15. Comparison of the first two natural frequencies (a-1 and a-2) of a cracked aluminium beam with different auxiliary masses and the relative deviation (b-1 and b-2) between the experimental and analytically predicted results: (———) predicted frequency, $m = 2$ kg, (– · – · –), predicted frequency, $m = 4$ kg, (—●—) experimental frequency, $m = 2$ kg, (– · ▲ – ·) experimental frequency, $m = 4$ kg; (a-1) and (b-1) for the first natural frequency, (a-2) and (b-2) for the second natural frequency.

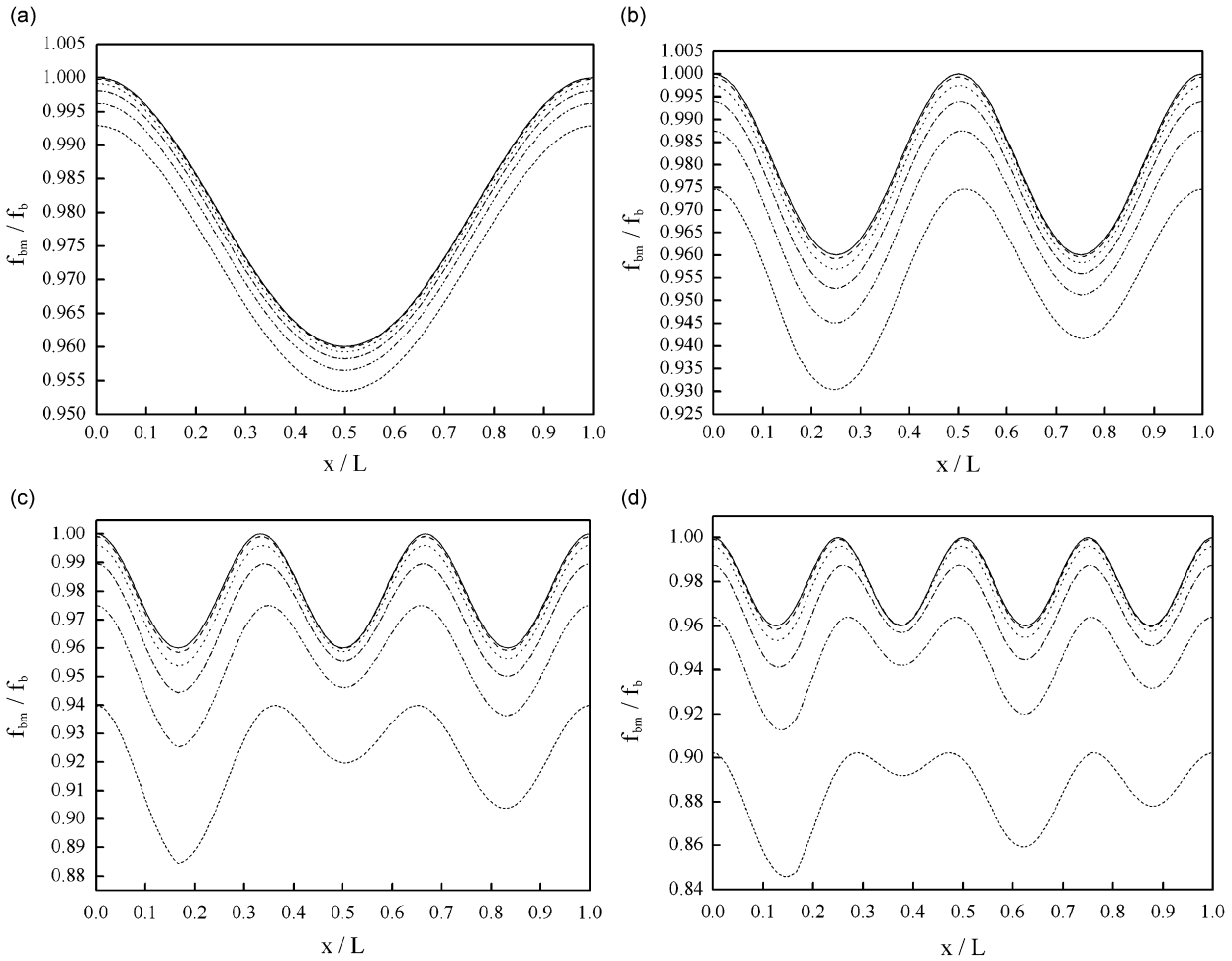

Fig. 16. Variation of the frequency ratio f_{bm}/f_b of the cracked beam ($l_c/L = 0.4$) with non-dimensional axial location x/L of the auxiliary mass ratio $m/M_b = 4.2\%$: (———) $h_c/H = 0$ (intact beam), (– – – –) $h_c/H = 10\%$, (· · · · ·) $h_c/H = 20\%$, (–·–·–·) $h_c/H = 30\%$, (–··–··–) $h_c/H = 40\%$, (·····) $h_c/H = 50\%$ for (a) mode 1, (b) mode 2, (c) mode 3, and (d) mode 4.

The frequency ratios decreased greatly if the crack is located at an antinodal position where the amplitude of the mode shape is largest. For example, mode 3 has an antinode at position $l_c/L = 2/12$. Therefore, large-differences in frequencies are observed at this antinodal position. Other very large differences in frequencies of mode 3 are observed at the other antinodal positions at $l_c/L = 6/12$ and $l_c/L = 10/12$. It should be observed that the differences in frequencies observed at $l_c/L = 10/12$ are similar to those observed at $l_c/L = 2/12$. Also, it is noted here that if the crack is exactly on the node of one mode, the variation of the frequency ratio of the cracked beam is almost the same as that of the intact beam. For example, from curve 7 in Fig. 17(b), which is the variation of the frequency ratio of the second mode of the beam with a crack located at the position of $l_c/L = 6/12$, is identical to curve 1, which is the variation of the frequency ratio of the second mode of the intact beam. For the same reason, curves 1 and 5 in Fig. 17(c) are identical while curves 1, 4 and 7 in Fig. 17(d) are overlapped.

It is obvious that if the beam-like structure is a symmetrical one, the curve of the variation of the frequency ratio of the structure with the roving mass will be also symmetrical. For example, it can be seen from Fig. 17 that all the curves of the variation of the frequency ratio of the intact beam with the roving mass are symmetrical. Also, all curves labelled '7' in Fig. 17(a)–(d) are symmetrical because the cracks are located at the centre of the beam and the structure is a symmetrical one. For the other cases, if the crack is not located at

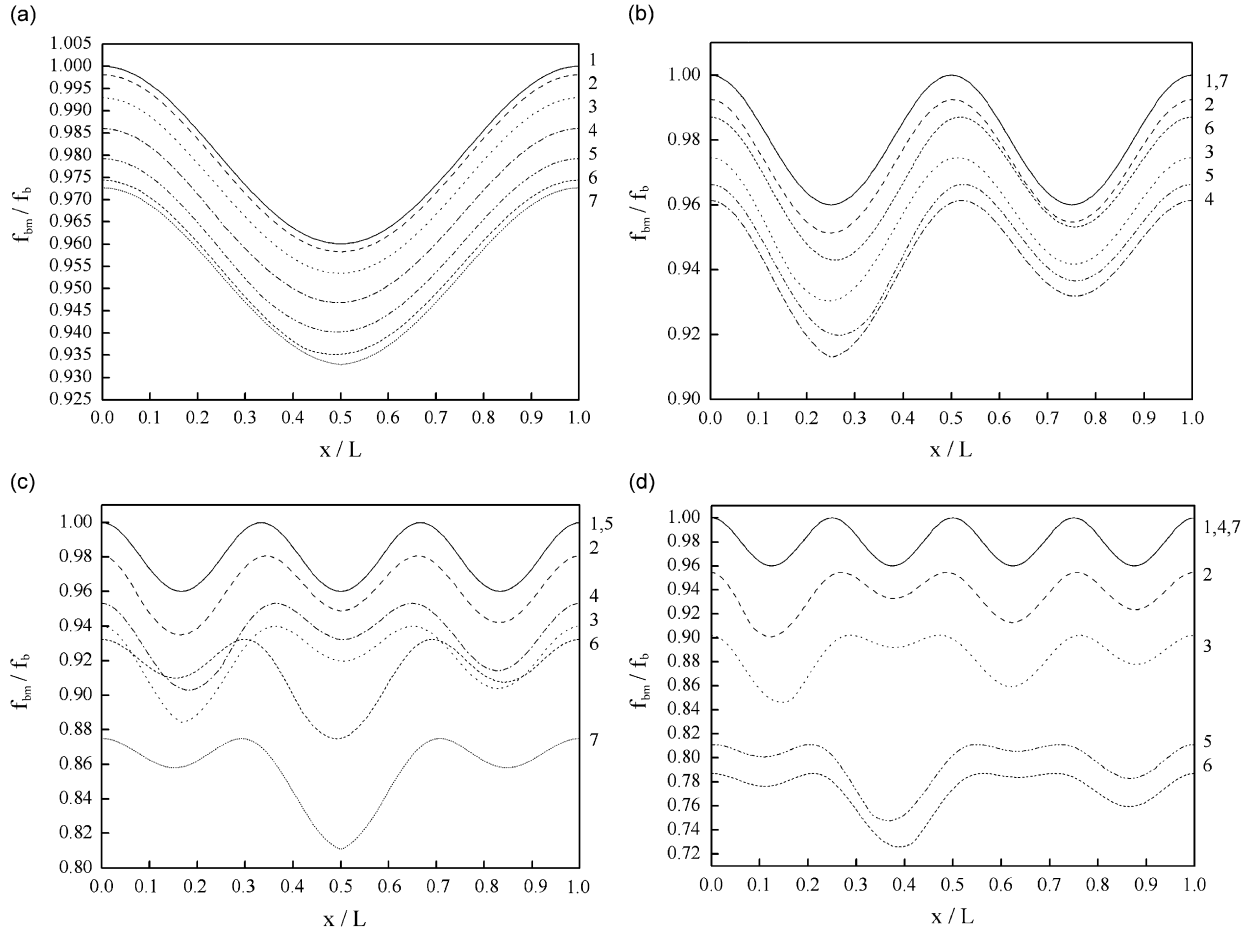

Fig. 17. Variation of the frequency ratio f_{bm}/f_b of the cracked beam ($h_c/H = 50\%$) with non-dimensional axial location x/L of the auxiliary mass ratio $m/M_b = 4.2\%$: (1) (————) intact beam, (2) (– – – –) $l_c/L = 1/12$, (3) (· · · · ·) $l_c/L = 2/12$, (4) (–·–·–·) $l_c/L = 3/12$, (5) (–··–··–) $l_c/L = 4/12$, (6) (·–·–·–·) $l_c/L = 5/12$, (7) (. . . . . .) $l_c/L = 6/12$ for (a) mode 1, (b) mode 2, (c) mode 3, and (d) mode 4.

the centre of the beam, the curves of the variation of the frequency ratio of the beam with the roving mass are asymmetrical, as can be seen from Fig. 17.

4.6. Combined effects of crack and roving mass

Fig. 18 shows the variation of the frequency ratio f_{bm}/f_b of an intact beam with non-dimensional axial location of the roving mass for different roving mass ratios. Six roving mass ratios are used, namely, $m/M_b = 0\%$, 10%, 20%, 30%, 40% and 50%. Because the intact simply supported beam is a symmetrical one, all the curves of the variation of the frequency ratio are symmetrical. It can be seen from Fig. 18 that when $m/M_b = 0\%$, no roving mass is added on the beam, the frequency ratio is 1. But when roving masses of ratios $m/M_b = 10$–50% are traversed along the length of the beam, Fig. 18 shows that the first four frequency ratios decrease in magnitude as the roving mass ratio increases. However, all the frequency curves remain symmetrical.

Fig. 19 shows the variation of the frequency ratio of the cracked beam with non-dimensional axial location of the roving mass for different roving mass ratios. In this case, the crack depth ratio and crack location ratio are, respectively, $h_c/H = 50\%$ and $l_c/L = 50\%$. Also the roving masses of ratios $m/M_b = 10$–50% are added. Comparing the results in Figs. 18 and 19, it is seen that the frequency ratios of modes 1 and 3 of the cracked

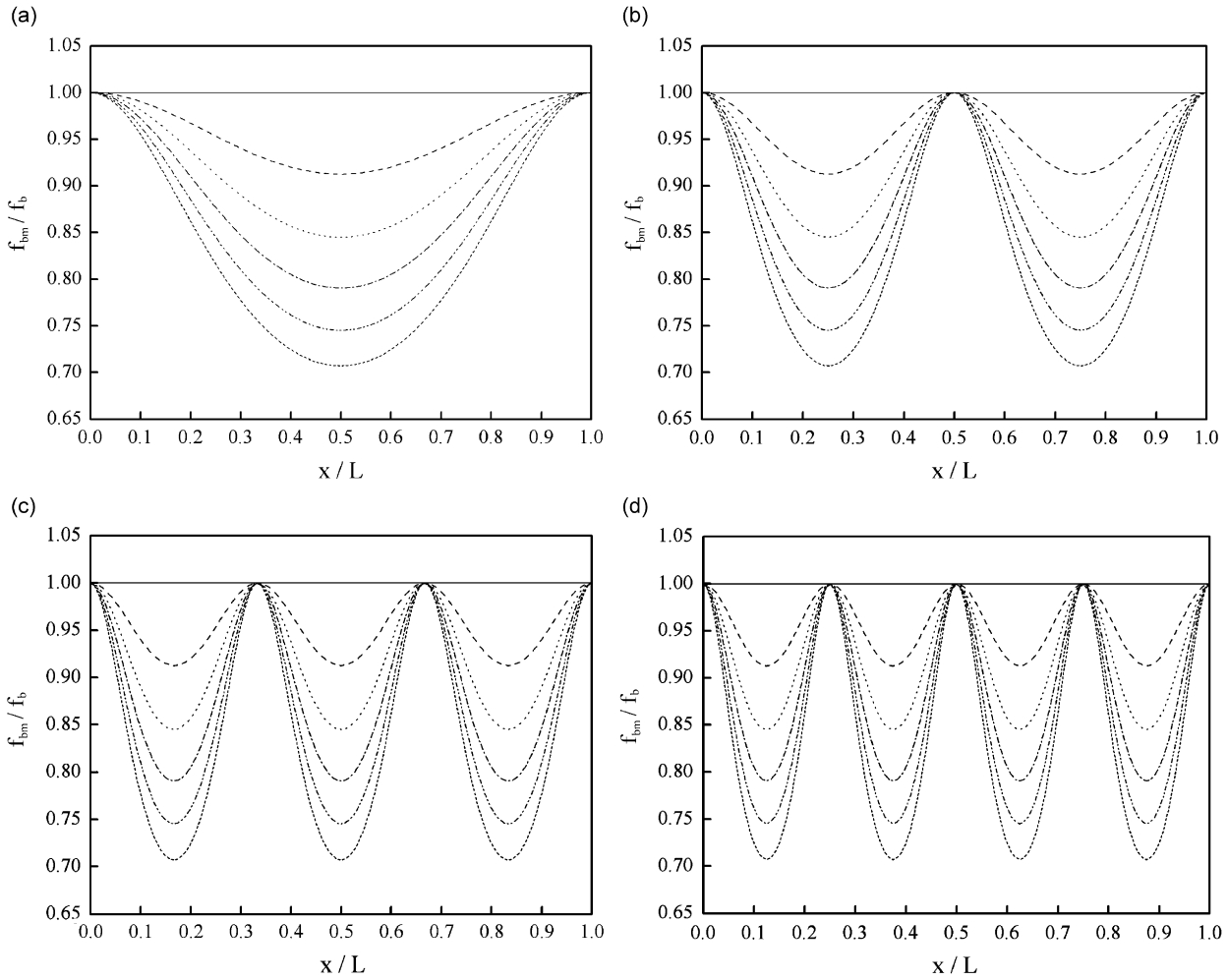

Fig. 18. Variation of the frequency ratio f_{bm}/f_b of an intact beam with non-dimensional axial location x/L of the auxiliary mass for different auxiliary mass ratios (m/M_b): (————) $m/M_b = 0\%$, (– – – –) $m/M_b = 10\%$, (· · · · · ·) $m/M_b = 20\%$, (–· – · – ·) $m/M_b = 30\%$, (–· · – · · –) $m/M_b = 40\%$, (· · · · · · · ·) $m/M_b = 50\%$, for (a) mode 1, (b) mode 2, (c) mode 3, and (d) mode 4.

beam are smaller than those of the intact beam with the same roving mass. This is due to the fact that the location of the crack at the centre of the beam coincides with the antinodal positions of modes 1 and 3. Also, since the crack is located at the centre of the beam, the structure is symmetrical. Therefore, all the curves in Fig. 19 are symmetrical.

As stated previously, if the crack is exactly on the node of one mode, the variation of the frequency ratio of the cracked beam is almost the same as that of the intact beam. Consequently, all curves in Fig. 19(b) and (d), which show the variation of the frequency ratios for modes 2 and 4 of the cracked beam with a roving mass, are the same as those in Fig. 18(b) and (d), respectively. The reason is that modes 2 and 4 have nodal positions at the centre of the beam (Fig. 20).

5. Concluding remarks

This paper presents an analytical method to evaluate natural frequencies of an arbitrary mode of a cracked beam-like structure with a stationary roving mass. The transverse deflection of the cracked beam is

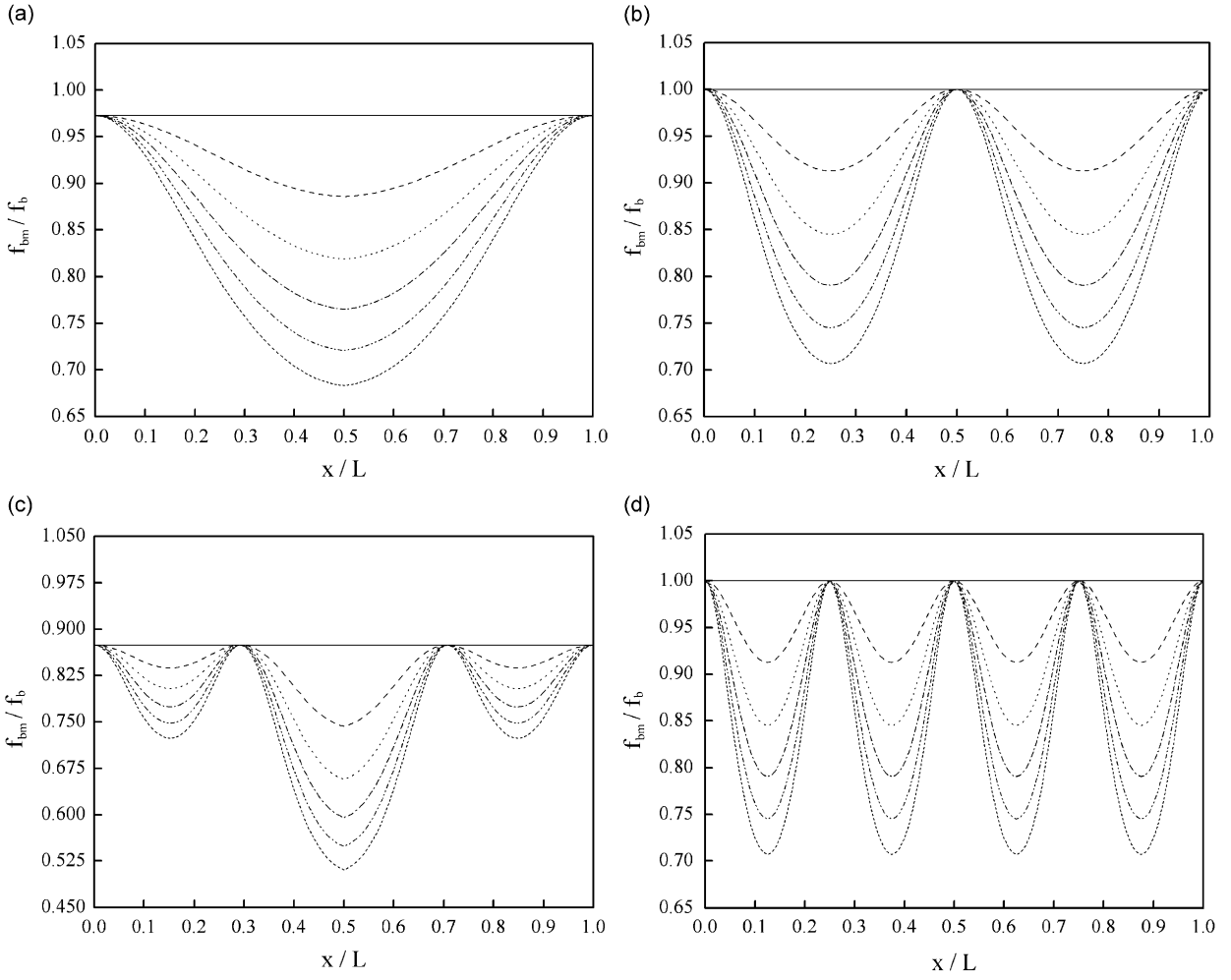

Fig. 19. Variation of the frequency ratio f_{bm}/f_b of the cracked beam ($l_c/L = 50\%$ and $h_c/H = 50\%$) with non-dimensional axial location x/L of the auxiliary mass for different auxiliary mass ratios (m/M_b): (———) $m/M_b = 0\%$, (– – – –) $m/M_b = 10\%$, (· · · · · ·) $m/M_b = 20\%$, (–· –· –·) $m/M_b = 30\%$, (–·· –·· –·) $m/M_b = 40\%$, (·····) $m/M_b = 50\%$, for (a) mode 1, (b) mode 2, (c) mode 3, and (d) mode 4.

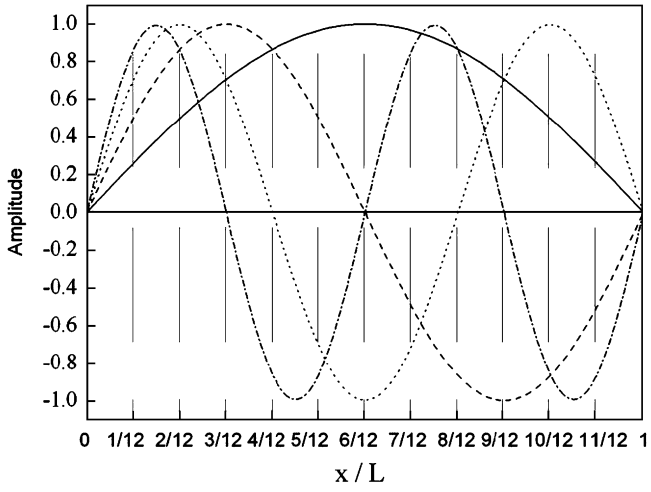

Fig. 20. The first four mode shapes of the simply supported beam: (———) first mode, (– – – –) second mode, (· · · · · ·) third mode, and (–· –· –·) fourth mode.

constructed by adding a polynomial function, which represents the effects of the crack, to the polynomial function which represents the response function of the intact beam. By means of the boundary and kinematics conditions, approximate closed-form analytical expressions are derived for the natural frequencies of arbitrary modes of transverse vibration of a simply supported cracked beam with a roving mass using the Rayleigh's method. Natural frequencies change due to the roving mass along the cracked beam, therefore the roving mass can provide additional spatial information for damage detection of the beam. The predicted frequencies have been shown to compare very well with those obtained using the FEM and the experimental results. The investigations on the effects of crack depth, crack location and the roving mass magnitude show that the natural frequencies of the cracked beam decrease as the crack depth increases and as the roving mass is traversed closer to the crack location. In a real application to damage detection using the roving mass, the magnitude of the mass should be limited to a low value to avoid destroying the beam-like structure itself.

It should be noted that the analytical method presented in this paper is valid under the consideration of the assumptions that the cracked beam does not include the effects of rotary inertia and shear deformation, that the BCs of the cracked beam are simply supported, and that the crack remains open during vibration. A future work on the method based on the use of the Timoshenko beam model, which includes the effects of rotary inertia and shear deformation, will be studied to provide a more accurate method for cracked beams with small span-to-height ratios.

Appendix A. Derivation of the first natural angular frequency

$$\begin{aligned} U_{\max} &= \frac{EI}{2}\left[\int_0^{l_c}\left(\frac{\mathrm{d}^2U_{c11}(x)}{\mathrm{d}x^2}\right)^2\mathrm{d}x+\int_{l_c}^{L}\left(\frac{\mathrm{d}^2U_{c21}(x)}{\mathrm{d}x^2}\right)^2\mathrm{d}x\right]+\frac{1}{2}\Delta\Theta\, M\\ &= \frac{EI}{2}\int_0^{l_c}\left[-D_1\left(\frac{\pi}{L}\right)^2\sin\left(\frac{\pi x}{L}\right)\right]^2\mathrm{d}x+\frac{EI}{2}\int_{l_c}^{L}\left[-D_1\left(\frac{\pi}{L}\right)^2\sin\left(\frac{\pi x}{L}\right)\right]^2\mathrm{d}x\\ &\quad+\frac{1}{2}\left[-\frac{D_1\pi^2HS(h_c/H)\sin\left((l_c\pi)/L\right)}{L^2}\right]\left[-\frac{D_1EI\pi^2\sin\left((l_c\pi)/L\right)}{L^2}\right]\\ &= \frac{D_1^2EI\pi^4\left[1+(H/L)S(h_c/H)(1-\cos\left((2l_c\pi)/L\right)\right]}{4L^3}, \end{aligned} \tag{A.1}$$

$$\begin{aligned} T_{\max} &= \frac{\rho A\omega^2}{2}\left[\int_0^{l_c}U_{c11}^2(x)\,\mathrm{d}x+\int_{l_c}^{L}U_{c21}^2(x)\,\mathrm{d}x\right]+\frac{1}{2}m\omega_1^2U_{c1}^2(l_m)\\ &= \frac{\rho A\omega^2}{2}\left\{\int_0^{l_c}\left[D_1\sin\left(\frac{\pi x}{L}\right)-D\frac{l_cW}{L^3}\left(1-\frac{L}{l_c}\right)S(h_c/H)\pi^2\sin\left(\frac{\pi l_c}{L}\right)x\right]^2\mathrm{d}x\right.\\ &\quad\left.+\int_b^{L}\left[D_1\sin\left(\frac{\pi x}{L}\right)+D\frac{l_cH}{L^2}S(h_c/H)\pi^2\sin\left(\frac{\pi l_c}{L}\right)\left(1-\frac{x}{L}\right)\right]^2\mathrm{d}x\right\}\\ &\quad+\frac{1}{2}m\omega_1^2U_{c1}^2(l_m)\\ &= \frac{1}{4}AD_1^2L\rho\omega_1^2\left\{1+2\left(\frac{H}{L}\right)S(h_c/H)\left[1-\cos\left(\frac{2l_c\pi}{L}\right)\right]\right.\\ &\quad\left.+\frac{\pi^4}{3}\left(\frac{H}{L}S(h_c/H)\right)^2\left[\left(\frac{l_c}{L}\right)^4-2\left(\frac{l_c}{L}\right)^3+\left(\frac{l_c}{L}\right)^2\right]\left[1-\cos\left(\frac{2\pi l_c}{L}\right)\right]\right\}\\ &\quad+\frac{1}{2}m\omega_1^2U_{c1}^2(l_m). \end{aligned} \tag{A.2}$$

By the Rayleigh's principle (form of the energy method), $T_{\max} = U_{\max}$. Therefore, equating Eqs. (A.1) and (A.2) gives

$$\omega_{c1}(n) = \left(\frac{\pi}{L}\right)^2 \sqrt{\frac{EI}{\rho A}} \left[\frac{1 + \frac{H}{L} S(h_c/H)\left[1 - \cos\left(\frac{2l_c\pi}{L}\right)\right]}{\left\{ \begin{array}{l} 1 + 2\left(\frac{H}{L} S(h_c/H)\right)\left[1 - \cos\left(\frac{2l_c\pi}{L}\right)\right] \\ + \frac{\pi^4}{3}\left(\frac{H}{L} S(h_c/H)\right)^2 \left[\left(\frac{l_c}{L}\right)^4 - 2\left(\frac{l_c}{L}\right)^3 + \left(\frac{l_c}{L}\right)^2\right]\left[1 - \cos\left(\frac{2\pi l_c}{L}\right)\right] \\ + \frac{2mU_{c1}^2(l_m)}{D_1 \rho A L} \end{array} \right\}} \right]^{1/2}. \tag{A.3}$$

Let

$$\eta = \left(\frac{H}{L}\right) S, \tag{A.4}$$

$$\gamma_1 = 1 - \cos(2\pi l_c/L), \tag{A.5}$$

$$\alpha_1'(n) = \frac{2mU_{c1}^2(l_m)}{D_1^2 \rho A L}, \tag{A.6}$$

$$l_m = n\,\Delta l, \quad n = 0, 1, 2, \ldots, \frac{L}{\Delta l} + 1, \tag{A.7}$$

$$\omega_1 = (\pi/L)^2 \sqrt{\frac{EI}{\rho A}}. \tag{A.8}$$

Substituting Eqs. (A.4)–(A.8) into Eq. (A.3), gives

$$\omega_{c1}(n) = \omega_1 \left[\frac{1 + \eta\gamma_1}{1 + 2\eta\gamma_1 + (\pi^4/3)\eta^2[(l_c/L)^4\gamma_1 - 2(l_c/L)^3\gamma_1 + ((l_c/L)^2\gamma_1)] + \alpha_1'(n)} \right]^{1/2}. \tag{A.9}$$

References

[1] A.D. Dimarogonas, Vibration of cracked structures: a state of the art review, *Engineering Fracture Mechanics* 55 (5) (1996) 831–857.

[2] O.S. Salawu, Detection of structural damage through changes in frequencies: a review, *Engineering Structures* 19 (1997) 718–723.

[3] X.T. Wang, C.C. Chang, L.C. Fan, Nondestructive damage detection of bridges: a status review, *Advances in Structural Engineering* 4 (2) (2001) 75–91.

[4] G. Zhou, L.M. Sim, Damage detection and assessment in fibre-reinforced composite structures with embedded fibre optic sensors: review, *Smart Materials and Structures* 11 (2002) 925–939.

[5] P.C. Chang, A. Flatau, S.C. Liu, Review paper: health monitoring of civil infrastructure, *Structural Health Monitoring* 2 (3) (2003) 257–267.

[6] E.P. Carden, P. Fanning, Vibration based condition monitoring: a review, *Structural Health Monitoring* 3 (4) (2004) 355–377.

[7] T.G. Chondros, A.D. Dimarogonas, Identification of cracks in welded joints of complex structures, *Journal of Sound and vibration* 69 (4) (1980) 531–538.

[8] T.G. Chondros, A.D. Dimarogonas, Dynamic sensitivity of structures to cracks, *Journal of Vibration, Acoustics, Stress and Reliability in Design* 111 (1989) 251–256.

[9] T.G. Chondros, The continuous crack flexibility model for crack identification, *Fatigue and Fracture of Engineering Materials & Structures* 24 (2001) 643–650.
[10] P. Cawley, R.D. Adams, The location of defects in structures from measurement of natural frequencies, *Journal of Strain Analysis* 14 (1979) 49–57.
[11] Y. Narkis, Identification of crack location in vibrating simply supported beams, *Journal of Sound and Vibration* 172 (1994) 549–558.
[12] A. Messina, I.A. Jones, Damage detection and localization using natural frequency change, *14th International Modal Analysis Conference*, Orlando, 1996, pp. 67–76.
[13] A. Messina, E.J. Williams, T. Contursi, Structural damage detection by sensitivity and statistical-based method, *Journal of Sound and Vibration* 216 (1998) 791–808.
[14] S. Christides, A.D.S. Barr, One dimensional theory of cracked Bernoulli–Euler beams, *International Journal of the Mechanical Sciences* 26 (1984) 639–648.
[15] T.G. Chondros, A.D. Dimarogonas, J. Yao, A continuous cracked beam vibration theory, *Journal of Sound and Vibration* 215 (1998) 17–34.
[16] J. Fernández-Sáez, L. Rubio, C. Navarro, Approximate calculation of the fundamental frequencies for bending vibrations of cracked beams, *Journal of Sound and Vibration* 225 (1999) 345–352.
[17] M.H.H. Shen, C. Pierre, Natural modes of Bernouilli–Euler beams with symmetric cracks, *Journal of Sound and Vibration* 138 (1990) 115–134.
[18] J. Fernández-Sáez, C. Navarro, Fundamental frequency of cracked beams in bending vibrations: an analytical approach, *Journal of Sound and Vibration* 256 (2002) 17–31.
[19] J.A. Loya, L. Rubio, J. Fernández-Sáez, Natural frequencies for bending vibrations of Timoshenko cracked beams, *Journal of Sound and Vibration* 29 (2006) 640–653.
[20] K.H. Low, An equivalent-center method for quick frequency analysis of beams carrying a concentrated mass, *Computers & Structures* 50 (1994) 409–419.
[21] G.B. Chai, K.H. Low, On the natural frequencies of beams carrying a concentrated mass, *Journal of Sound and Vibration* 160 (1993) 161–166.
[22] M.A. De Rosa, C. Franciosi, M.J. Maurizi, On the dynamic behaviour of slender beams with elastic ends carrying a concentrated mass, *Computers & Structures* 58 (1996) 1145–1159.
[23] K.H. Low, Comparisons of experimental and numerical frequencies for classical beams carrying a mass in-span, *International Journal of Mechanical Sciences* 41 (1999) 1515–1531.
[24] K.H. Low, A modified Dunkerley formula for eigenfrequencies of beams carrying concentrated masses, *International Journal of Mechanical Sciences* 42 (2000) 1287–1305.
[25] K.H. Low, On the methods to derive frequency equations of beams carrying multiple masses, *International Journal of Mechanical Sciences* 43 (2001) 871–881.
[26] K.H. Low, Frequencies of beams carrying multiple masses: Rayleigh estimation versus eigenanalysis solutions, *Journal of Sound and Vibration* 268 (2003) 843–853.
[27] T.G. Chondros, A.D. Dimarogonas, J. Yao, Vibration of a beam with a breathing crack, *Journal of Sound and Vibration* 239 (1) (2001) 57–67.
[28] M.A. Mahmoud, M.A. Abou Zaid, Dynamic response of a beam with a crack subject to a moving mass, *Journal of Sound and Vibration* 256 (4) (2002) 591–603.
[29] H.P. Lin, S.C. Chang, Forced responses of cracked cantilever beams subjected to a concentrated moving load, *International Journal of Mechanical Sciences* 48 (2006) 1456–1463.
[30] S.S. Rao, *Mechanical Vibration*, fourth ed., Addison-Wesley Publishing Company, 2004.
[31] A.D. Dimarogonas, *Vibration for Engineers*, second ed., Prentice-Hall Engineering, 1996.
[32] W.T. Thomson, *Theory of Vibration with Applications*, fourth ed., Chapman & Hall, London, 1993.
[33] F.S. Tse, I.E. Morse, R.T. Hinkle, *Mechanical Vibrations*, second ed., Allyn & Bacon, Boston, 1978.
[34] H. Tada, P.C. Paris, G.R. Irwin, *The Stress Analysis of Cracks Handbook*, third ed., The American Society of Mechanical Engineers, New York, 2000.
[35] H. Salarieh, M. Ghorashi, Free vibration of Timoshenko beam with finite mass rigid tip load and flexural–torsional coupling, *International Journal of Mechanical Sciences* 48 (2006) 763–779.
[36] ABAQUS, *User's Manual, Version 6.2*, Hibbitt, Karlsson & Sorensen Inc., Providence, RI, 2001.